AD-A259 433

Defense Nuclear Agency
Alexandria, VA 22310-3398

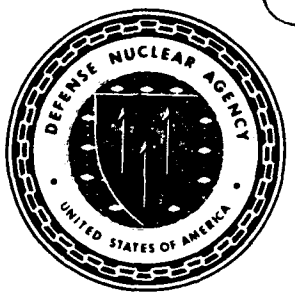

DNA-TR-90-171

Analysis of Prolate Spheroidal Shell under Undex Load

David S. Nokes
Charles Stark Draper Laboratory, Inc.
555 Technology Square
Cambridge, MA 02139

DTIC
ELECTE
JAN 14 1993
S D

December 1992

Technical Report

CONTRACT No. DNA 001-89-C-0006

Approved for public release;
distribution is unlimited.

93-00849
5698

Destroy this report when it is no longer needed. Do not return to sender.

PLEASE NOTIFY THE DEFENSE NUCLEAR AGENCY, ATTN: CSTI, 6801 TELEGRAPH ROAD, ALEXANDRIA, VA 22310-3398, IF YOUR ADDRESS IS INCORRECT, IF YOU WISH IT DELETED FROM THE DISTRIBUTION LIST, OR IF THE ADDRESSEE IS NO LONGER EMPLOYED BY YOUR ORGANIZATION.

DISTRIBUTION LIST UPDATE

This mailer is provided to enable DNA to maintain current distribution lists for reports. (We would appreciate your providing the requested information.)

NOTE:
Please return the mailing label from the document so that any additions, changes, corrections or deletions can be made easily.

☐ Add the individual listed to your distribution list.

☐ Delete the cited organization/individual.

☐ Change of address.

NAME: _____

ORGANIZATION: _____

OLD ADDRESS	CURRENT ADDRESS
_____	_____
_____	_____
_____	_____

TELEPHONE NUMBER: ( ) _____

DNA PUBLICATION NUMBER/TITLE	CHANGES/DELETIONS/ADDITIONS, etc.) *(Attach Sheet if more Space is Required)*
_____	_____
_____	_____
_____	_____

DNA OR OTHER GOVERNMENT CONTRACT NUMBER: _____

CERTIFICATION OF NEED-TO-KNOW BY GOVERNMENT SPONSOR (if other than DNA):

SPONSORING ORGANIZATION: _____

CONTRACTING OFFICER OR REPRESENTATIVE: _____

SIGNATURE: _____

CUT HERE AND RETURN

DEFENSE NUCLEAR AGENCY
ATTN: TITL
6801 TELEGRAPH ROAD
ALEXANDRIA, VA 22310-3398

DEFENSE NUCLEAR AGENCY
ATTN: TITL
6801 TELEGRAPH ROAD
ALEXANDRIA, VA 22310-3398

REPORT DOCUMENTATION PAGE

Form Approved
OMB No. 0704-0188

Public reporting burden for this collection of information is estimated to average 1 hour per response, including the time for reviewing instructions, searching existing data sources, gathering and maintaining the data needed, and completing and reviewing the collection of information. Send comments regarding this burden estimate or any other aspect of this collection of information, including suggestions for reducing this burden, to Washington Headquarters Services, Directorate for Information Operations and Reports, 1215 Jefferson Davis Highway, Suite 1204, Arlington VA 22202-4302, and to the Office of Management and Budget, Paperwork Reduction Project (0704-0188), Washington, DC 20503.

1. AGENCY USE ONLY *(Leave blank)*	2. REPORT DATE	3. REPORT TYPE AND DATES COVERED
	921201	Technical 890301-900831

4. TITLE AND SUBTITLE
Analysis of Prolate Spheroidal Shell under Undex Load

5. FUNDING NUMBERS
C -DNA 001-89-C-0006
PE-62715H
PR-RS
TA-RF
WU-DH055790

6. AUTHOR(S)
David S. Nokes

7. PERFORMING ORGANIZATION NAME(S) AND ADDRESS(ES)
Charles Stark Draper Laboratory, Inc.
555 Technology Square
Cambridge, MA 02139

8. PERFORMING ORGANIZATION REPORT NUMBER

9. SPONSORING/MONITORING AGENCY NAME(S) AND ADDRESS(ES)
Defense Nuclear Agency
6801 Telegraph Road
Alexandria, VA 22310-3398
SPSD/Tsai

10. SPONSORING/MONITORING AGENCY REPORT NUMBER
DNA-TR-90-171

11. SUPPLEMENTARY NOTES

This work was sponsored by the Defense Nuclear Agency under RDT&E RMC Code B4662D RS RF 00097 SPSD 4300A 25904D.

12a. DISTRIBUTION/AVAILABILITY STATEMENT
Approved for public release;
distribution is unlimited.

12b. DISTRIBUTION CODE

13. ABSTRACT *(Maximum 200 words)*

This effort was an attempt to verify a newly developed closed-formed solution to the transient response of a submerged prolate spheroidal shell structure due to underwater explosive shock loading. Numerical solutions were attempted for three test cases ranging from a sphere to an elongated spheroidal shell approximating the shape of a submarine.

Results for the spherical case were exactly the same as for the previously reported theory which is restricted to spheres. The results for the elongated spheroidal shells were in error, with the magnitude of the errors increasing as the amount of elongation increased. The errors appear to result from truncation of the infinite series solutions. As a result, useful results could not be obtained using currently reasonable computer resources.

14. SUBJECT TERMS
Spheroidal Shell
Underwater Shock
Fluid-Solid Interaction
Undex Load
Shell Theory

15. NUMBER OF PAGES
54

16. PRICE CODE

17. SECURITY CLASSIFICATION OF REPORT	18. SECURITY CLASSIFICATION OF THIS PAGE	19. SECURITY CLASSIFICATION OF ABSTRACT	20. LIMITATION OF ABSTRACT
UNCLASSIFIED	UNCLASSIFIED	UNCLASSIFIED	SAR

NSN 7540-01-280-5500

Standard Form 298 (Rev. 2-89)
Prescribed by ANSI Sta. 239-18
298-102

CLASSIFIED BY:

N/A since Unclassified.

DECLASSIFY ON:

N/A since Unclassified.

EXECUTIVE SUMMARY

The objective of this effort was to verify a newly developed closed-form solution to the transient response of a submerged prolate spheroidal shell structure under the loading of an underwater shock.

The closed-form solution for the response of a spherical shell had been previously developed (Ref. 1, 2). Numerical results had been generated for a particular test case. These results had been verified by an underwater shock testing program (Ref. 3).

The current research has attempted to extend these results to the prolate spheroidal shell case. A prolate spheroidal shell with a major diameter approximately 10 times the minor diameter is a reasonable approximation to the shape of a modern submarine. A closed-form solution for this case would be useful to cross check numerical or finite element solutions for the underwater shock response of submarine hulls.

Graduate student research sponsored by the The Charles Stark Draper Laboratory, Inc., herein after known as Draper, under Independent Research and Development (IR&D) funding had developed the theoretical basis for the solution to this problem (Ref. 4). The purpose of this effort was to obtain specific numerical solutions for comparison with other numerical methods or test data.

Numerical solutions were attempted for three test cases. The first case was an almost perfect sphere. This case produced exactly the same results as previously reported for the sphere, thus providing a first cross check of the theory.

The second test case was an egg shaped prolate spheroidal shell. This case gave good results for the natural frequencies of the shell in vacuum, but did not give reasonable results of the shock loading. The third case was a submarine shaped prolate spheroidal shell. For this case, all the numerical results were obviously in error.

The theory appears to be complete and correct. However, the answers are in the form of infinite series solutions. In some cases, the series are cross coupled, making for an infinite square matrix of terms. For practical solution with currently reasonable computer resources, the cross-coupling terms must be dropped and the series truncated at a reasonable number of terms. Unfortunately, this results in incorrect answers. In the future, increased computer power may make this solution useful in an engineering sense. However, at this time the method can not be used to solve practical problems.

Since reasonable numerical solutions could not be obtained for high eccentricity geometries using the new closed-form theory, we were unable to compare the new theory with experimental or finite element results.

Editorial Note: The above view does not necessarily agree with that of Dr. Janet Jones-Oliveira who developed the theory as presented in Reference 4.

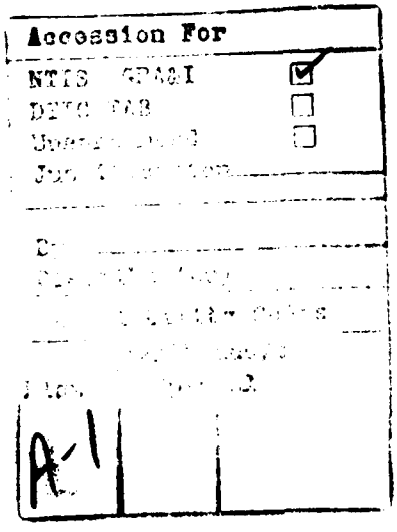

CONVERSION TABLE

angstrom	1.000 000 X E -10	meters(m)
atmosphere	1.013 25 X E +2	kilo pascal (kPa)
bar	1.000 000 X E +2	kilo pascal (kPa)
barn	1.000 000 X E -28	meter^2 (m^2)
British thermal unit (thermochemical)	1.054 350 X F +3	joule (J)
calorie (thermochemical)	4.184 000	joule (J)
cal(thermochemical)/cm^2	4.184 000 X E -2	mega joule/m^2 (MJ/m^2)
curie	3.700 000 X E +1	•giga becquerel (GBq)
degree (angle)	1.745 329 X E -2	radian (rad)
degree Fahrenheit	t_g = (t° f + 459.67)/1.8	degree kelvin (K)
electron volt	1.602 19 X E -19	joule (J)
erg	1.000 000 X E -7	joule (J)
erg/second	1.000 000 X E -7	watt (W)
foot	3.048 000 X E -1	meter (m)
foot-pound-force	1.355 818	joule (J)
gallon (U.S. liquid)	3.785 412 X E -3	meter^3 (m^3)
inch	2.540 000 X E -2	meter (m)
jerk	1.000 000 X E +9	joule (J)
joule/kilogram (J/kg) (radiation dose absorbed)-	1.000 000	Gray (Gy)
kilotons	4.133	terajoules
kip (1000 lbf)	4.448 222 X E +3	newton (N)
kip/inch^2 (ksi)	6.894 757 X E +3	kilo pascal (kPa)

CONVERSION TABLE (Continued)

ktap	1.000 000 X E +2	newton-second/m^2 ($N\text{-}s/m^2$)
micron	1.000 000 X E -6	meter (m)
mil	2.540 000 X E -5	meter (m)
mile (international)	1.609 344 X E +3	meter (m)
ounce	2.834 952 X E -2	kilogram (kg)
pound-force (lbs aviordupois)	4.448 222	newton (N)
pound-force-inch	1.129 848 X E -1	newton-meter (N-m)
pound-force/inch	1.751 268 X E +2	Newton/meter (N/m)
pound-force/$foot^2$	4.788 026 X E -2	kilo pascal (kPa)
pound-force/$inch^2$ (psi)	6.894 757	kilo pascal (KPa)
pound-mass (lbm avoirdupois)	4.535 924 X E -1	kilogram (kg)
pound-mass-$foot^2$ (moment of inertia)	4.214 011 X E -2	kilogram-$meter^2$ (kg - m2)
pound-mass/$foot^3$	1.601 846 X E +1	kilogram/$meter^3$ (kg/m^3)
rad (radiation dose absorbed)	1.000 000 X E -2	**Gray (Gy)
roentgen	2.579 760 X E -4	coutomb/kilogram (C/kg)
shake	1.000 000 X E -8	second (s)
slug	1.459 390 X E +1	kilogram (kg)
torr (mm Hg, 0°C)	1.333 22 X E -1	kilo pascal (kPa)

* The becquerel (Bq) is the SI unit of radioactivity; 1 Bq = 1 event/s.

** The Gray (Gy) is the SI unit of absorbed radiation

TABLE OF CONTENTS

LIST OF ILLUSTRATIONS

LIST OF TABLES

SECTION 1

INTRODUCTION

Structural acoustics is an area of mathematical physics which addresses the coupled fluid-solid interaction between a structure and the fluid in which it is immersed. In fluid-solid interaction problems, the analysis of the response of structures is coupled through the boundary conditions to the propagation of energy in the fluid environment. It is incorrect to analyze an immersed structure independently of the fluid medium, to analyze the fluid independently of a structure in its midst, and then to superimpose the solutions. These problems require the simultaneous solution of the coupled field equations for both media (Ref. 4, Chapter 1).

Because of the coupled nature of the problem, very few closed form solutions have been developed. The problem of the shock response for a sphere in water was previously solved by Draper (Ref. 1, 2). Numerical results were developed for a spherical shell structure which Draper was developing for a different program. The numerical results were then compared with actual shock test results (Ref. 3). The agreement was excellent.

Encouraged by these results, we attempted to extend the analysis to a prolate spheroidal shell geometry. Unfortunately, this simple change in the geometry caused a very large increase in the difficulty of the solution. Without the aid of computers, solution would be practically impossible.

However, computer programs are now available to help with the algebra involved with manipulating the complex series expressions which result from attempts to solve this problem in closed form. In particular, the DOE-MACSYMA program was used extensively to help in reducing the equations to more reasonable forms.

SECTION 2

THEORETICAL DEVELOPMENT

The theoretical development of the equations is given in detail in Jones-Oliveira (Ref. 4). We will present here only a brief summary of the steps involved.

The objective is to analyze the transient response of a prolate spherical shell structure which has been externally loaded by an end-on explosive waterborne shock wave. The intention is to analyze the effects of giving up one level of geometric symmetry (two degrees of symmetry for the prolate spheroid versus three degrees of symmetry for the previous sphere analysis) (Ref. 4, Chapter 2).

Several simplifying assumptions are necessary to formulate a solution to this problem. It is assumed that linear acoustic wave theory is sufficient to describe the propagation of the pressure field in the water. This is a reasonable assumption except very near the explosive charge. Koiter-Sanders-Budiansky theory for thin elastic shells is used for the formulation of the shell structure internal strain and kinetic energy expressions (Ref. 4, Chapter 2). It is assumed that the fluid remains in contact with the shell at all times (no cavitation). This will be true for reasonable explosive loads except very near the surface.

With these assumptions, the problem is linear. One set of differential equations describes the motion of the fluid. A second set of differential equations describes the motion of the shell structure. The two sets of equations are coupled by the requirement that the normal velocity and the pressure load are matched at all times at the fluid-solid interface. The problem has thus been reduced to finding the solution to these equations, a far from trivial task.

The problem is formulated in a prolate spheroidal coordinate system. The temporally and spatially dependent shell displacement and fluid pressure fields are expressed modally in terms of the prolate spheroidal angular functions of the first kind and a new set of prolate spheroidal radial functions of the first and third kinds. The prolate spheroidal angular functions are shown to be solutions of both the acoustic wave equation, which governs the fluid behavior, and the shell equilibrium equations. They are not the eigenfunctions of the coupled fluid-structure problem. However, the solutions are exact within the limits of using a finite numbers of terms of a infinite series to represent the solution (Ref. 4, Abstract).

The prolate spheroidal special functions are expressed in terms of classical spherical harmonics: Specifically, Legendre polynomials and modified spherical Bessel functions of the first and third kinds (Ref. 4, Abstract).

The mathematical physics governing the symmetry order two prolate spheroidal problem is fundamentally different from that of the symmetry order three spherical problem previously solved. The underlying geometric differences are at the root of the modal coupling, which is compounded by the fluid-solid interaction at the interface. The totally uncoupled spherical response is a limiting case of the more general and fully coupled prolate spheroidal response (Ref. 4, Chapter 2).

The modal coupling, which is not present in the spherical case, is the primary limitation to obtaining practical solutions. If the coupling were not present, it would be reasonable to carry a large number of terms in the series solutions. If the series converged very rapidly, it would not be too difficult to solve the fully coupled problem using only a few terms in the series. Unfortunately, it appears that neither is true.

DOE-MACSYMA was used extensively to determine the solution to this problem. The capabilities of the symbolic computer code have been demonstrated to be invaluable for parametric analysis (Ref. 4, Abstract). Unfortunately, the complexity of the resulting coupled functions is overwhelming, even with DOE-MACSYMA. It became obvious that simplifications were imperative to achieve solutions within the limitations of DOE-MACSYMA and reasonable total computer time. It was necessary to estimate the relative magnitudes of each of the coupling terms to determine when terms could be neglected. These simplifications must be considered judgement calls.

The coupling terms are more significant as the aspect ratio is increased. In principal, this is not a limitation. As the aspect ration increased, one would just carry more terms in the solution. In practice, this is subject to limitations:

1. Numerical precision of the calculations must also be increased to avoid round-off error.

2. Computer programs have size limits. In particular, DOE-MACSYMA can handle large, but not unlimited, problems. This analysis was stretching its limits.

3. Computers have become faster and less expensive. However, problems which are attempted have also grown. This problem might have been possible to solve to higher accuracy by the use of much larger computer resources, but it would have been prohibitively expensive to try.

SECTION 3

NUMERICAL RESULTS[1]

3.1 PHYSICAL AND GEOMETRIC PARAMETERS.

The physical constants are given in Table 1 on page 6. The fluid is taken to be fresh water, and the shell material is steel.

The acoustic loading is that resulting from a sixty-pound spherical charge of HBX-1 located at a stand-off distance (S.O.D.) of 25 feet from the nose of the prolate spheroids. The peak external pressure[2] of the incident pressure wave is given by

$$P = 22{,}347.6\left(\frac{W^{\frac{1}{3}}}{S.O.D.}\right)^{1.144} \tag{3.1}$$

and the exponential decay constant associated with the explosive charge is given by

$$\tilde{\beta} = 0.056\, W^{\frac{1}{3}}\left(\frac{W^{\frac{1}{3}}}{S.O.D.}\right)^{-0.247} \tag{3.2}$$

where the explosive charge weight W is given in *lbs* and the stand-off distance *S.O.D.* is given in *ft*. The peak external pressure is expressed in terms of $\frac{lbs}{in^2}$ and the exponential decay constant is expressed in terms of *ms*.

---

1 Numerical calculations are presented for three representative prolate spheroidal geometries. The first case models a "nearly spherical" geometry and is offered as verification of the correctness of the code by comparing the results to the sperical analog. The second case models a "rounded-off football." Preliminary results are offered for a third case which models a "submarine-like" structure. The numerical complexities are enormous. Limitations and comments are noted.

2 Formulas for the explosive characteristics are given in Jones-Oliveira (Ref. 4, Chapter 5.4).

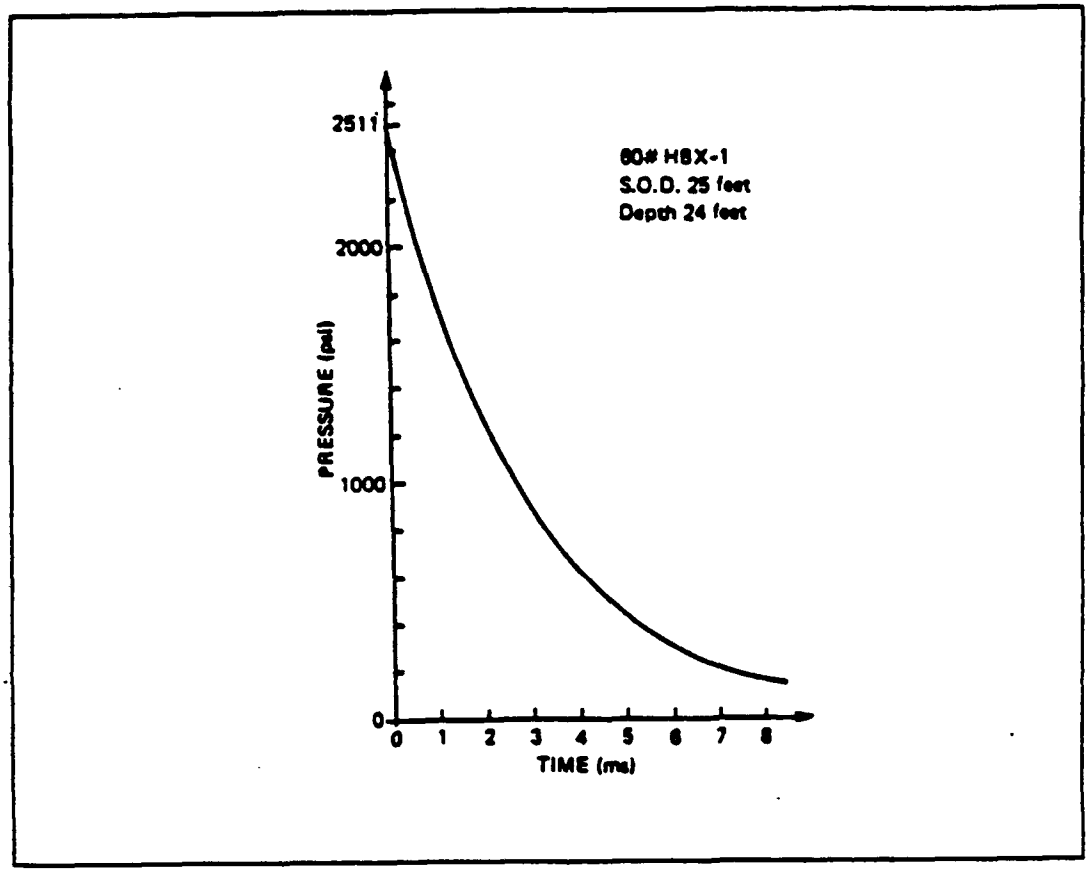

Figure 1. Pressure versus time curve.

Table 1. Physical constants: This table provides the physical material properties used to generate the numerical examples.

SYMBOL	DEFINITION	VALUE
$\tilde{\beta}$	exponential decay constant	0.3466 ms
c_f	sound velocity in fluid	1498 $\frac{m}{s}$
c_s	sound velocity in shell	5404 $\frac{m}{s}$
C^2	nondimensionalized sound speed squared	13.0
E	Young's modulus	$2.11 \times 10^{10} \frac{kg}{m^2}$
ν	Poisson's ratio	0.30
P	peak external pressure given 60 # of HBX-1 at 25 ft S.O.D.	1,883,966 $\frac{kg}{m^2}$
Π	nondimensionalized peak pressure	8.2406×10^{-3}
ρ_f	density of water	$1.0188 \times 10^2 \frac{kg\text{-}s^2}{m^4}$
ρ_s	density of shell	$7.9385 \times 10^2 \frac{kg\text{-}s^2}{m^4}$
$\rho_f g$	specific weight of water	999.1 $\frac{kg}{m^3}$
$\rho_s g$	specific weight of shell	7785 $\frac{kg}{m^3}$

The geometric parameters associated with each of the three cases are given in Table 2 on page 9. In each case, a specific shell geometry was selected and sized, and the shell thickness was determined to ensure a neutrally buoyant body.

The neutral buoyancy condition is defined such that the mass of the fluid displaced by the prolate spheroid must equal the mass of the prolate spheroidal shell. The volume of a prolate spheroid is given by $V = \frac{4}{3}\pi ab^2 = \frac{4}{3}\pi\xi\left(\xi^2-1\right)$ (Ref. 4, Chapter 2.4.1). Clearly, the neutral buoyancy condition is a function of the nondimensionalized mass ratio, but it is also a function of the eccentricity. The nondimensionalized shell thickness may be determined by solving the following cubic equation.

$$999.1\left[\left(\xi_o+\frac{h}{2}\right)^3-\left(\xi_o+\frac{h}{2}\right)\right]$$

$$=7785\left[\left(\xi_o+\frac{h}{2}\right)^3-\left(\xi_o+\frac{h}{2}\right)-\left(\xi_o-\frac{h}{2}\right)^3+\left(\xi_o-\frac{h}{2}\right)\right] \qquad (3.3)$$

The remaining geometric parameters are then nondimensionalized as per (Ref. 4, Chapter 2.7). Note that the nondimensionalizations of time differ for each of the three cases; therefore, so must the scaled values of the incident pressure exponential decay constant β.

Case I: Model of a nearly spherical shell. The prolate spheroid has a low aspect ratio of 1.005 with $\xi_o = 10.0$. The pseudo-spherical parameters were selected to facilitate comparison to the spherical shell which was modeled, tested and presented in Jones-Oliveira (Ref. 2). It should be noted that the parameters are not identically those cited in Jones-Oliveira (Ref. 2); therefore, the results will be different. The shell and fluid properties differ slightly; and the shell thickness was determined to ensure neutral buoyancy.

Case II: Model of an intermediate aspect ratio geometry. Specifically, the aspect ratio is $\sqrt{2}$ with $\xi_o\sqrt{2}$ also. The parameters were selected, for comparison purposes, to match as closely as possible those of Pauwelussen (Ref. 7) and Nemergut & Brand (Ref. 6).

Case III: Model of a submarine-like structure. The prolate spheroid has a high aspect ratio of 10.0 and $\xi_o = 1.005$. In particular, the geometry is similar to a small submersible currently being developed at The Charles Stark Draper Laboratory.

Numerical results are also presented for a sphere which differs only slightly from the pseudo-spherical problem. Its geometric parameters are those given for Case I with the following exceptions: [1] the dimensional semifocal length is zero, $\tilde{f} = 0$; [2] the semiminor axis length is equal to the semimajor axis length, $\tilde{b} = \tilde{a}$; and [3] the semimajor axis length is equal to the limiting value, $\xi_o\tilde{f} = \tilde{a}$.

Table 2. Geometric parameters: This table provides the geometric parameters defining the three illustrative examples. Case I refers to the low aspect ratio example, Case II refers to the intermediate aspect ratio example, and Case III refers to the high aspect ratio example.

	CASE I	CASE II	CASE III
ξ_o	10.0000	1.4142	1.005
$\tilde{f}$	0.0323 m	1.4142 m	10.9182 m
$\tilde{a}$	0.3239 m	2.0000 m	10.9728 m
$\tilde{b}$	0.3222 m	1.4142 m	1.0932 m
$\tilde{h}$	0.0147 m	0.0549 m	0.0074 m
h	4.5469×10^{-2}	0.0275	6.7440×10^{-4}
AR	1.0050	1.4142	10.0375
e	0.1000	0.7071	0.995
$\frac{\tilde{h}^2}{12\tilde{f}^2}$	1.7229×10^{-2}	1.2554×10^{-4}	3.9×10^{-8}
M	2.8224	4.6761	189.4994
τ	4,642.9251 t	749.0 t	136.5194 t
β	1.6091	0.2596	0.0473
$\omega_n\,(hertz)$	$736.07319\Omega_n$	$119.20705\Omega_n$	$21.72774\Omega_n$

3.2 FREE VIBRATIONS OF PROLATE SPHEROIDS.

The first step in verifying the DOE-MACSYMA coding of the analysis was to compute the free in vacuo vibrations of the three representative prolate spheroids. Included are the *couplings* of the coefficients associated with the first eight Legendre polynomials. The spherical results are presented for comparison purposes. The nondimensionalized results are tabulated in Table 3 on page 12 and the dimensionalized frequencies are tabulated in Table 4 on page 14.

It is noted that the in vacuo natural frequencies of the pseudo-spherical prolate spheroid, i.e., Case I, for which $\xi = 10.0$ are within 1% of those computed for a sphere using the same parameters. However, one would expect the frequencies of the sphere to be slightly higher than those of the prolate spheroid. The discrepancies may be explained by the truncation of the infinite series representations of the prolate spheroidal angular functions expressed in terms of Legendre polynomials and/or by numerical errors and/or by omission of the expansion coefficients.

Agreement of the first few modes of Case II, for which $\xi = \sqrt{2}$, is remarkable. Nemergut & Brand (Ref. 6) computed an identical frequency for the lower branch of mode 2. In their paper, they compare their own results with those of Shiraishi & DiMaggio (Ref. 8) and Silbiger & DiMaggio (Ref. 9).

The results for Case III for which $\xi_2 = 1.005$, have to be considered somewhat suspect. The reasons for concern are: [1] the lowest odd frequency is not close enough to zero; and [2] the branches cross each other. Clearly, the rigid body translation, for which $m = 1$, should have a zero root. Normalization by the lowest "nonzero" frequency reveals cause for concern. Regarding the crossing of the branches, it is not known whether or not these results are correct. Several options for further investigation are: [1] increase the precision; [2] increase the number of modes that are allowed to couple; and/or [3] include the expansion coefficients in the analysis.[3] None of these suggestions is numerically trivial; however, the matter will be addressed further.

---

[3] As yet, the expansion coefficients in the numerics are all taken to be one. The assumption is that this dependence will ultimately be absorbed into the time-dependent generalized displacements as per (Ref. 4, Chapter 2.6.5).

It should be noted that there are, in fact, two branches; i.e., two natural frequencies associated with each mode number. Please refer to Figure 2 on page 13, which plots the dimensional frequencies as a function of mode number for Cases I & II. This phenomenon is an inherent characteristic of axisymmetric shell structures. The simultaneous solution of the homogeneous system of partial differential equations, which governs the normal and tangential deflections of shells of revolution, reduces to the solution of a quartic equation; specifically, it is bi-quadratic. Except for the pure breathing mode $m = 0$, there result two sets of nontrivial roots to the frequency determinant resulting in a bifurcation into a lower branch and an upper branch (Ref. 5, Chapter 8). The $m = 0$ is a special case; it has only a single complex-conjugate pair of roots because $u_o \equiv 0$.

The lower branch appears to contain the $\frac{\tilde{h}^2}{12\tilde{\rho}^2}$ parameter and is, therefore, sensitive to bending stiffness. On the other hand, the upper branch is relatively insensitive to bending stiffness. If one were to model only the extensional vibrations of the prolate spheroidal shell, which would imply that the $\frac{\tilde{h}^2}{12\tilde{\rho}^2}$ terms were omitted, then the frequencies on the lower branch would be too low but the frequencies on the upper branch would not be affected appreciably.

Finally, all of the even (odd) normal displacements are coupled to all of the even (odd) tangential displacements. Therefore, it is not possible, a priori, to discern which frequency (lower or upper branch) is associated with which displacement. It is conjectured that the lower branch may be dominated by the tangential displacements.

Table 3. Nondimensionalized in vacuo natural frequencies.

	SPHERE	PROLATE SPHEROID		
		Case I	Case II	Case III
mode	r	$\xi_0 = 10.0$	$\xi_0 = \sqrt{2}$	$\xi_0 = 1.005$
1	0.0	0.0	0.0049	2.7448
2	2.5325	2.5492	3.7592	7.7304
3	3.0252	3.0470	4.6356	12.9879
4	3.2799	3.3039	4.9566	17.9642
5	3.5125	3.5385	5.2955	23.4785
6	3.8030	3.8311	5.5944	28.4777
7	4.1922	4.2232	6.2635	37.3266
8	4.7012	4.7358	6.6211	36.9838
0	5.8138	5.8332	7.1347	41.6152
1	7.1210	7.1544	9.5473	39.1475
2	9.8168	9.8457	12.3497	44.4057
3	13.1101	13.1445	15.7277	48.1471
4	16.5785	16.6207	19.5272	52.5743
5	20.1094	20.1602	23.5383	73.3820
6	23.6685	23.7281	27.6355	81.2022
7	27.2426	27.3113	32.8058	198.7833
8	30.8255	30.9032	37.2074	218.9494

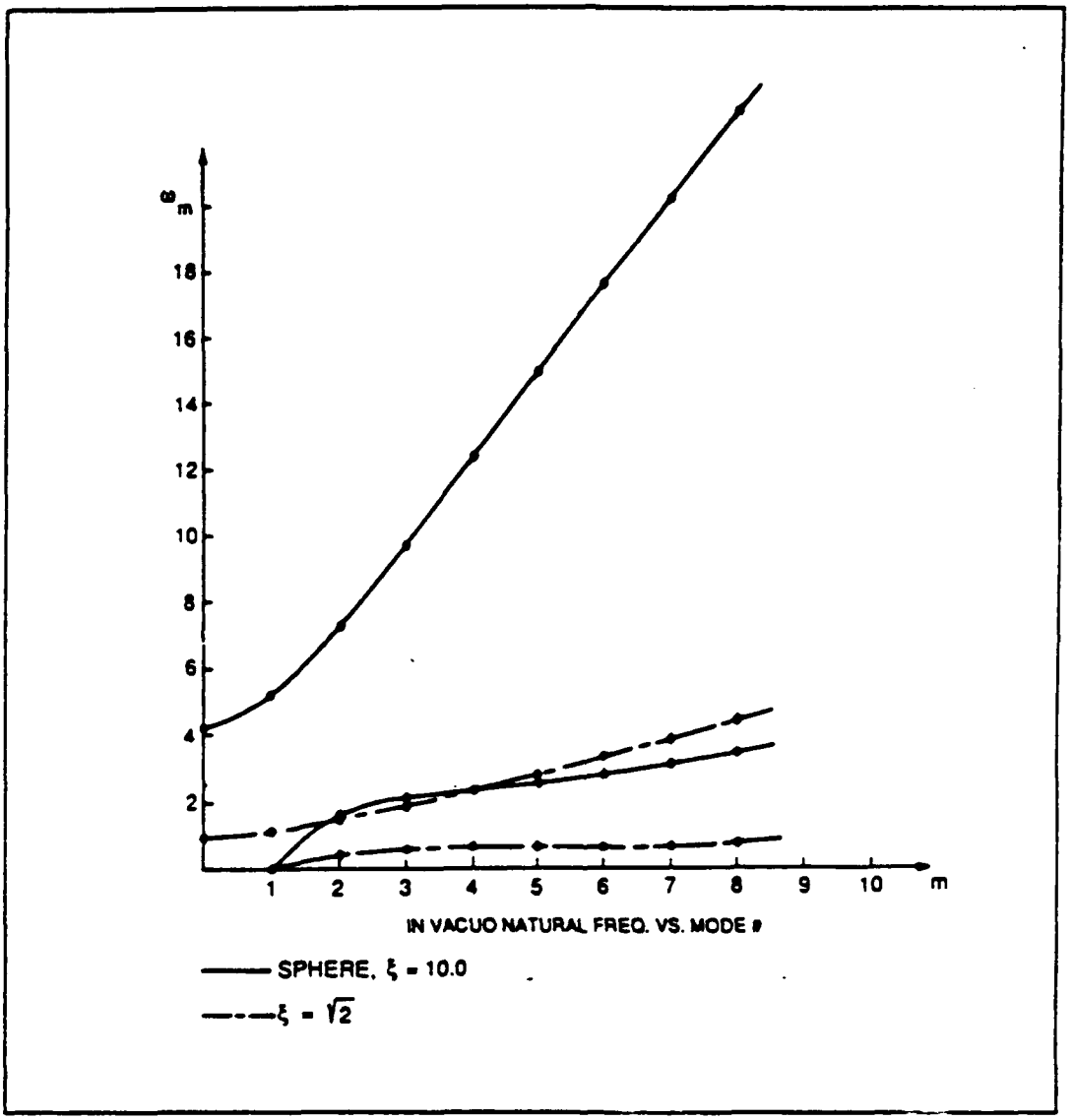

Figure 2. Dimensional Frequency versus mode number.

Table 4. Dimensional in vacuo natural frequencies (kilohertz).

	SPHERE	PROLATE SPHEROID		
		Case I	Case II	Case III
mode	r	$\xi_0 = 10.0$	$\xi_0 = \sqrt{2}$	$\xi_0 = 1.005$
1	0.0	0.0	5.8412×10^{-4}	0.0596
2	1.8639	1.8764	0.4481	0.1680
3	2.2265	2.2428	0.5526	0.2822
4	2.4140	2.4319	0.5909	0.3903
5	2.5852	2.6046	0.6313	0.5101
6	2.7990	2.8200	0.6669	0.6188
7	3.0854	3.1086	0.7467	0.8109
8	3.4601	3.4859	0.7893	0.8036
0	4.2789	4.2937	0.8720	0.9042
1	5.2411	5.2662	1.1381	0.8506
2	7.2252	7.2472	1.4722	0.9648
3	9.6491	9.6753	1.8749	1.0461
4	12.2018	12.2341	2.3278	1.1423
5	14.8005	14.8394	2.8059	1.5944
6	17.4200	17.4656	3.2943	1.7643
7	20.0506	20.1031	3.9107	4.3191
8	22.6876	22.7470	4.4354	4.7573

3.3 FLUID-LOADED VIBRATIONS.

In order to solve the even-even/odd-odd *coupled* equations for the fluid-loaded natural frequencies, it is necessary to simplify the equations. Here, the emphasis is on the "coupling" of the coefficients in the differential equations resulting from the Legendre polynomials representation. The trimming procedure is as follows:

1. Inspect the coefficients of each displacement appearing in the left-hand side of each of the modal equations given by (Ref. 4, 3.5.2a & 3.5.2b). Normalize the coefficients by the n^{th} coefficient of the displacement in the n^{th} equation. Let each normalized coefficient which is less than 0.0001 be set to 0.0. Allow an additional order of magnitude for each power of s (since the observed range of s satisfies $|s| < 20$).

2. Note that the coupling terms at the fluid-solid interface appearing on the right-hand side of equation (Ref. 4, 3.5.2a) (see also Ref. 4, 3.3.5.4) have a factor of $b_{ni} \times b_{nm}$. Each of these coefficients drops off rapidly as the mode numbers increase, so their products drop off even faster. Practically, this means that the inner summation in the numerator of (Ref. 4, 3.3.5.4) is not infinite; in fact, in most cases, only the diagonal elements survive the trimming procedure. In other words, only the $(b_{nm})^2$ terms usually survive.

3. When necessary and appropriate, back-substitute the solutions for the lower modes into the equations for the higher modes to solve for the higher modes.

These simplifications are necessary in order to compute the solution effectively. Otherwise, the order of the polynomials which must be solved exceeds the capabilities of the root solvers. For example, consider Case I for which $\xi_o = 10$. Without these simplifications, the order of the polynomial for solving the coupling of w_0, u_2, w_2, u_4, and w_4 is 64 and the DOE-MACSYMA ALLROOTS solver was only able to fund 14 of the roots. The polynomials become ill-conditioned.

It was verified that the roots are quite stable against this trimming procedure. For the smaller problem, which models the the most significant cross-coupling, specifically that associated with the lowest modes (w_0, u_2 and w_2), the roots moved by less than 1% with these simplifications. This smaller problem could be solved exactly and the results were used for the verification.

The characteristic roots are presented in the form

$$s = -\sigma \pm \Omega i$$

where s = Laplace variable

$-\sigma$ = tenuation

Ω = nondimensionalized damped natural frequency.

The first few roots for Case I, for which $\xi_o = 10.0$, are

m = 0: $w_0, u_0 \equiv 0$

$s = -1.940$

$s = -1.366 \pm 5.400i$

m = 1: w_1, u_1

$s = 0$

$s = -1.526 \pm 0.918i$

$s = -0.887 \pm 6.830i$

m = 2: w_2, u_2

$s = -1.097$

$s = -1.940$

$s = -3.052$

$s = -1.9101 \pm 2.455i$

$s = -0.1306 \pm 1.785i$

$s = -2.692 \pm 1.779i$

$s = -0.403 \pm 9.701i$

3.4 SHOCK-LOADED VIBRATIONS.

The characteristic roots for the shock-loaded problem are identical to the roots given for the fluid-loaded homogeneous problem with the addition of a root associated with the shock. Specifically, there is an additional real root s = -1.609.

The nondimensionalized normal and tangential displacements for the shock-loaded submerged shell are plotted as a function of nondimensionalized time. The dimensional deflections may be determined from the nondimensionalized values by multiplying by the $\xi_0\tilde{f}$ factors for the given geometry: Case I for which $\xi_0 = 10.0, \xi_0\tilde{f} = 0.323$; Case II for which $\xi_0 = \sqrt{2}, \xi_0\tilde{f} = 2.0$; and Case III for which $\xi_0 = 1.005, \xi_0\tilde{f} = 10.97$

Similar conversions may be used to obtain the physical dimensional velocities and accelerations. Refer to Table 5 on page 18 as necessary to relate nondimensionalized time τ to real time t.

Table 5. Nondimensionalized time versus real time (ms).

τ	Case I $\xi = 10.0$	Case II $\xi = \sqrt{2}$	Case III $\xi = 1.005$
0	0.0	0.0	0.0
1	0.215	1.335	7.325
2	0.431	2.670	14.650
3	0.646	4.005	21.975
4	0.862	5.341	29.300
5	1.077	6.676	36.625
10	2.154	13.351	73.250
15	3.231	20.027	109.875
20	4.308	26.702	146.500
25	5.385	33.378	183.124
30	6.461	40.053	219.749
35	7.538	46.729	256.374
40	8.615	53.405	292.999
45	9.692	60.080	329.624
50	10.769	66.756	366.248
60	12.923	80.107	439.498
70	15.077	93.458	512.748
80	17.231	106.809	585.997
90	19.384	120.160	659.247
100	21.538	133.511	732.497
110	23.692	146.863	805.763
120	25.846	160.214	878.996
130	28.000	173.565	952.246
140	30.153	186.916	1025.495
150	32.307	200.267	1098.745

3.4.1 Case I: Low Aspect Ratio.

Figure 3 on page 21 through Figure 16 on page 34 are DOE-MACSYMA-generated plots of the normal and tangential generalized displacements (i.e., the time-dependent amplitudes), normal and tangential physical displacements, velocities and accelerations for the low aspect ratio geometry in response to the specified underwater explosion.

The following observations were made.

- The rigid-body generalized displacements (modal time-dependent amplitudes), w_1, and u_1, indicate a finite displacement of the shell. This may be explained as follows. Recall that the generalized forces are the superposition of the incident, scattered and radiated pressure waves in the fluid. The incident shock wave imparts a force onto the prolate spheroidal shell and continues past the shell. Scattered energy is reflected off the shell back into the fluid. Radiated energy is also put back into the fluid due to the motion of the shell through the fluid, which can also re-load the structure. The loss of energy to the fluid, once the exponentially decaying incident shock wave has passed the prolate spheroid $(\tau > 2)$, damps the motion of the shell as it moves through the fluid resulting in the finite displacement.

- It is also noted that $\max(w_2) >> \max(w_0)$. This means that w_2 is strongly coupled to w_0 but not vice versa. The equations coupling w_0, u_2, and w_2 reveal that w_0 has both of the roots for $m = 0$ and the fourth root for $m = 2$, which points out a strong coupling to u_2 . This can be deduced because this fourth $m = 2$ root is the extra root associated with u_2, which is predicted by the analysis and comparison to the spherical problem.

- $\max(w_2) >> \max(w_0)$, $\max(w_4), \cdots$ and $\max(w_3) >> \max(w_5)$, $\max(w_7), \cdots$

- μ_n drops off rapidly as n increases.

- As the mode number increases, the couplings become negligible.

- As time progresses, the displacements can be seen to damp out and then to re-excite as the fluid and shell motions exchange their energy through the kinematic boundary conditions at the fluid-solid interface.

- The number of modes required to model the response adequately was determined by examining the accelerations, rather than by considering just the relative magnitudes of the displacement coefficients. It was determined that the acceleration contributed by the 7^{th} mode was less than 10% of the total acceleration contributed by modes $m = 0 - 6$. A better criterion could be established by examining the conservation of energy of the system. Acceleration information is of keen interest to experimental engineers because these predictions can be verified directly using accelerometers.

The shell strains, as defined by (Ref. 4, 3.1.1.5), and strain rates are presented in Figure 17 on page 35 through Figure 20 on page 38. Again, the strain information is of interest to experimental engineers because strain gauge readings are easily obtained. Comparisons of predicted values versus empirical data may be accomplished using the square root sum of the squares.

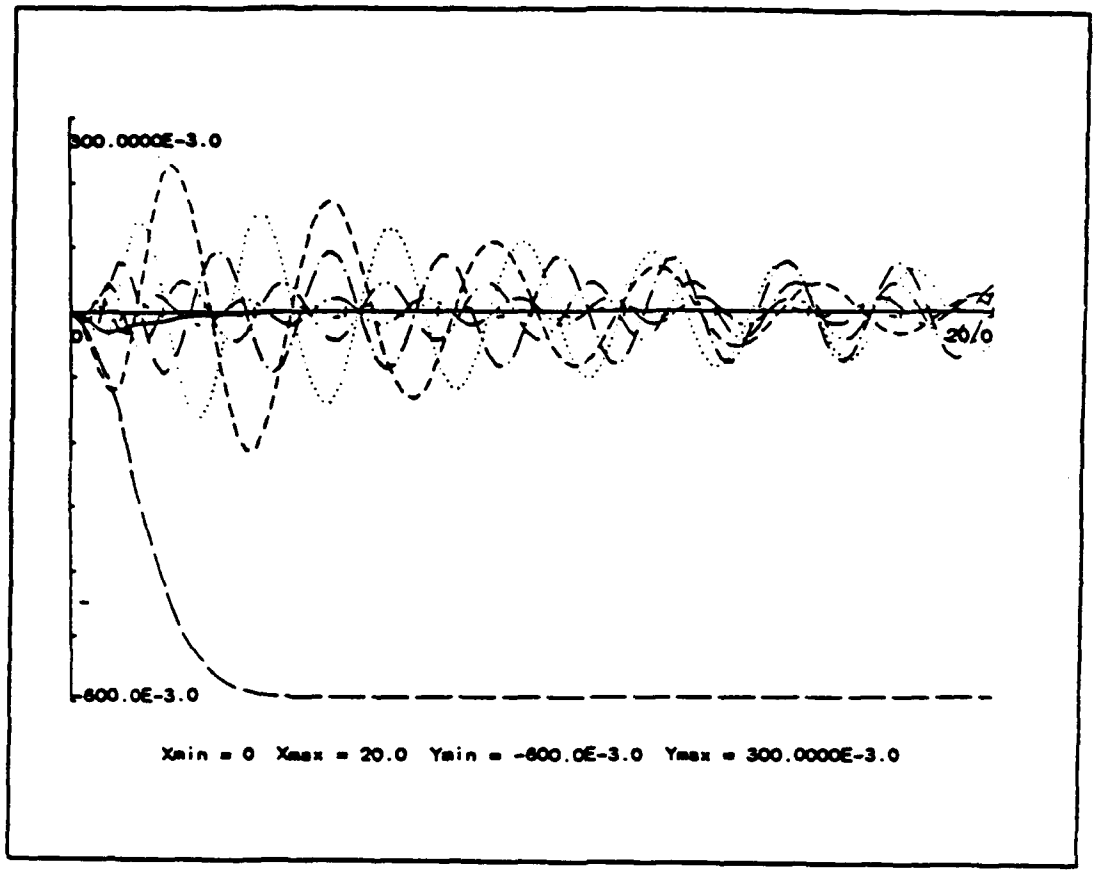

Legend

W_0 W_1 W_2 W_3 W_4 W_5 W_6 W_7

Figure 3. Modal time-dependent normal amplitudes for m = 0 - 7: With the exception of component m=1, the generalized displacements return to their original equilibrium position. However, the m = 1 contribution results in a finite displacement of the shell.

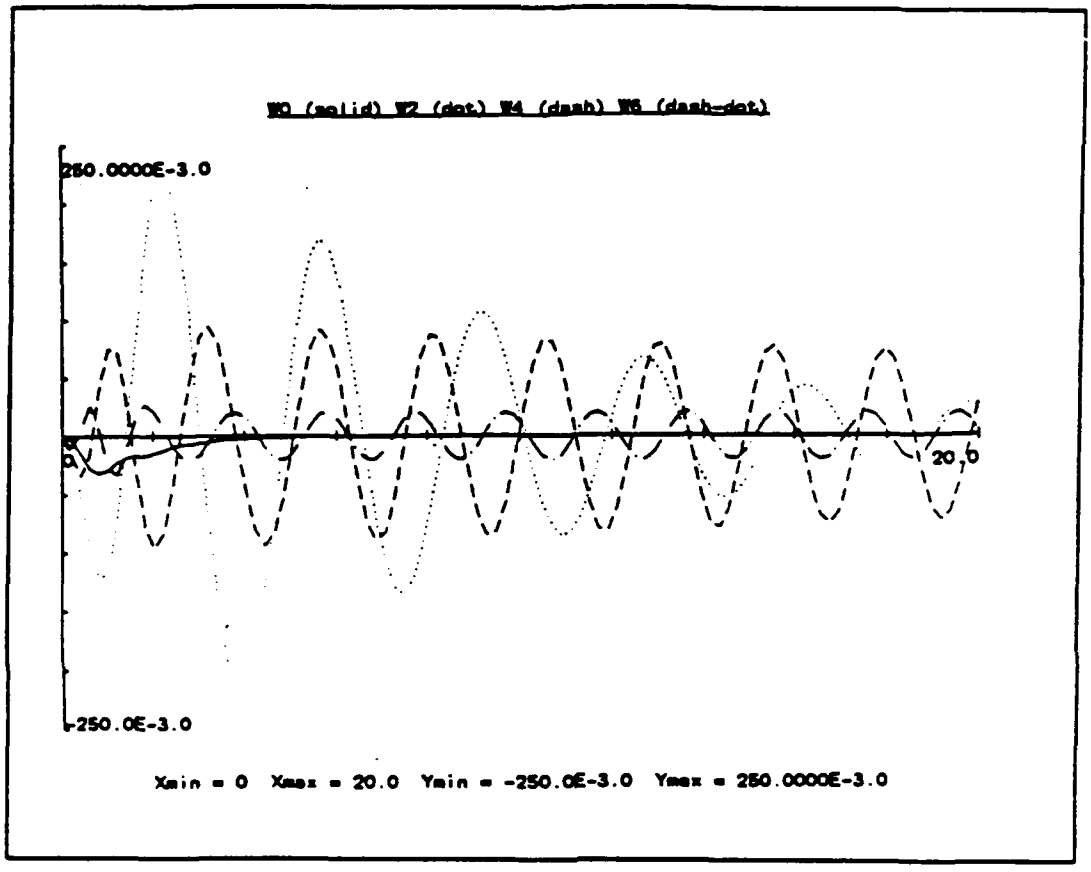

Figure 4. Transient normal deflection coefficients for even m = 0 - 6: Note that the m = 2 mode has the most significant amplitude. This explains its strong coupling to the lower even modes.

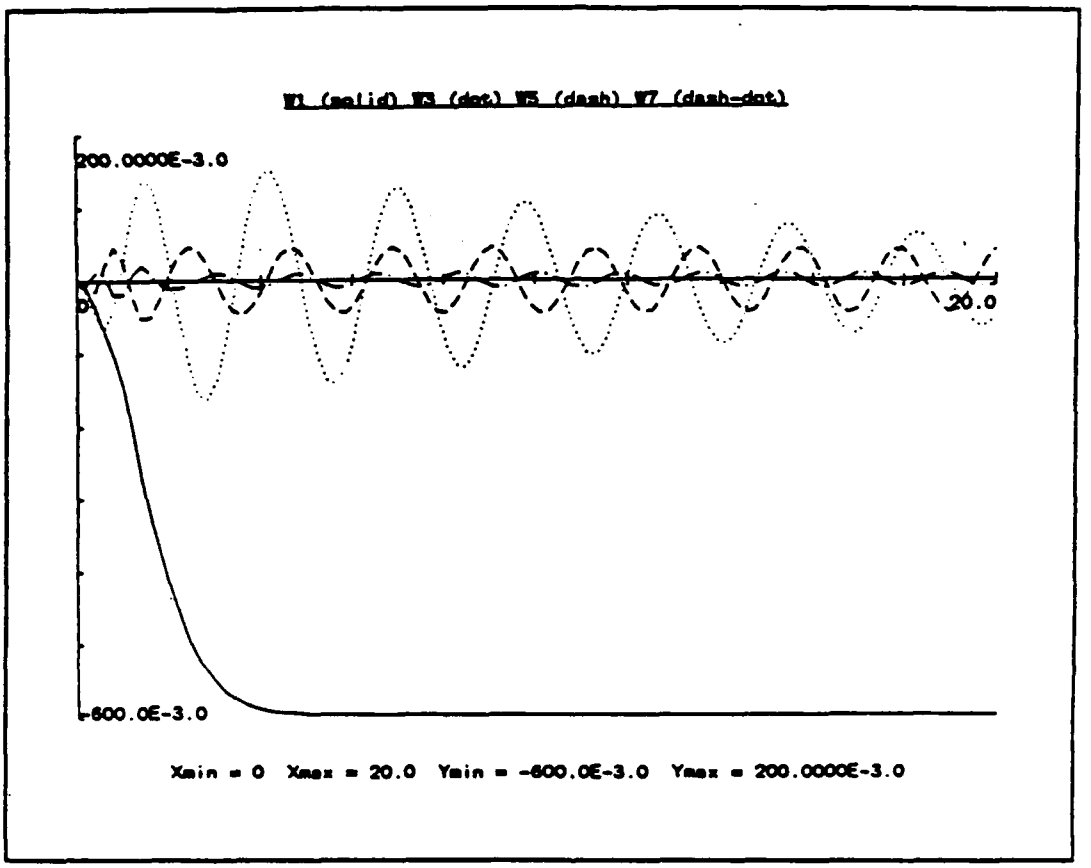

Figure 5. Transient normal deflection coefficients for odd m = 1 - 7: The m = 1 mode finite displacement reflects the transfer of energy from the shell to the fluid in the form of radiation.

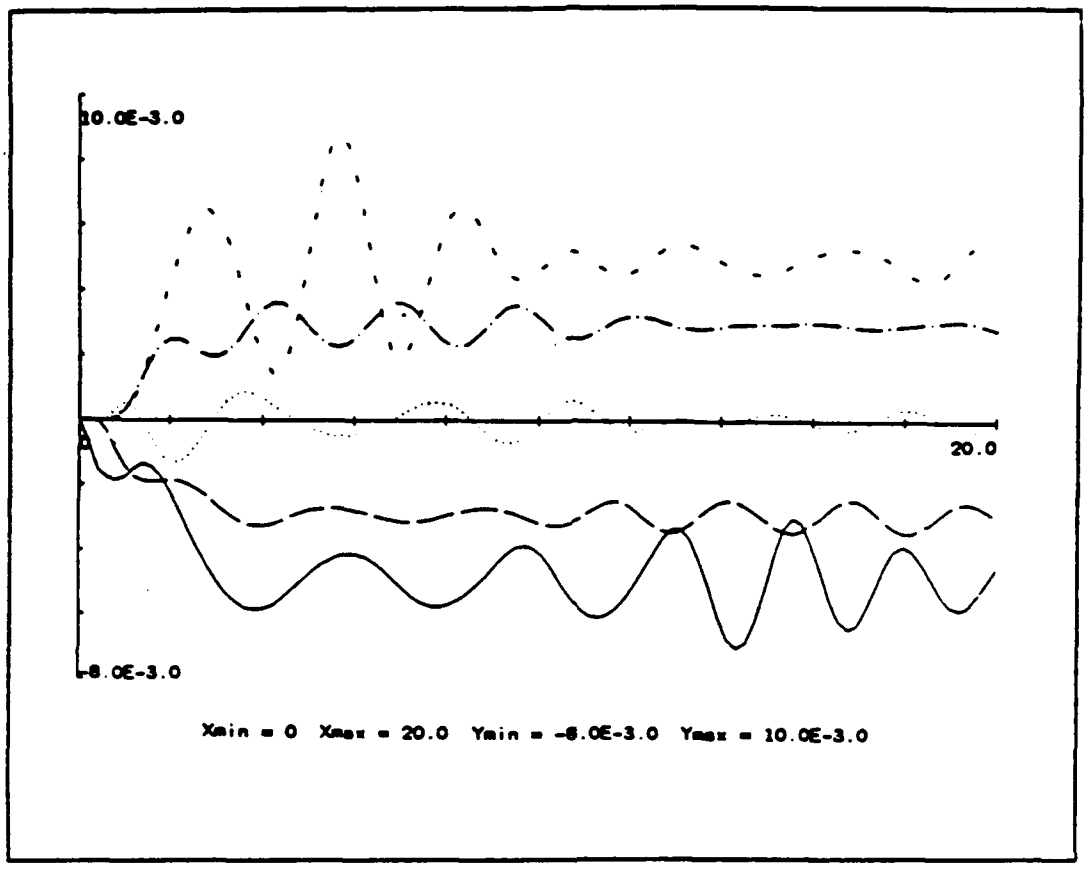

Legend

η= + 1.0
η= + 0.6
η= 0.0
η= - 0.6
η= - 1.0

Figure 6. Early-time normal displacements at five locations on the shell: The positions vary from the nose to the back side relative to the shock.

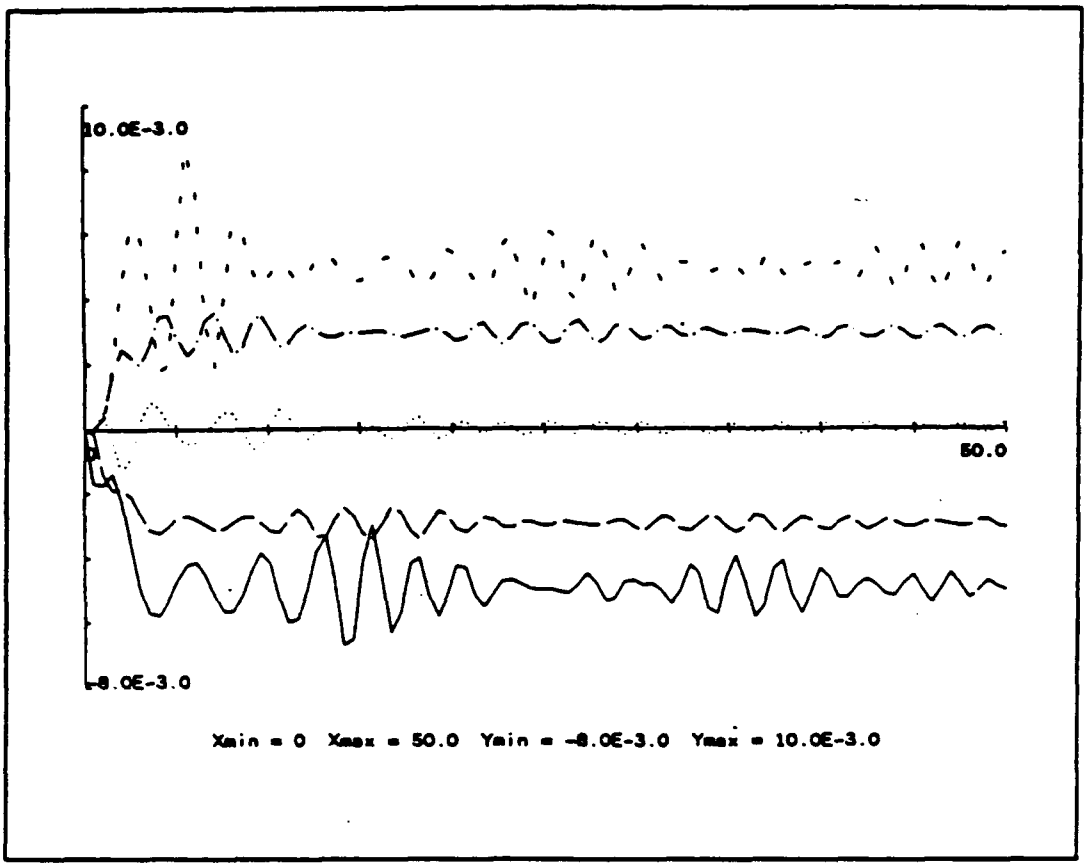

Legend

$\eta = +1.0$
$\eta = +0.6$
$\eta = 0.0$
$\eta = -0.6$
$\eta = -1.0$

Figure 7. Longer-time normal displacements at five locations on the shell: Note the oscillation of the displacement amplitudes—first dying out and then re-exciting.

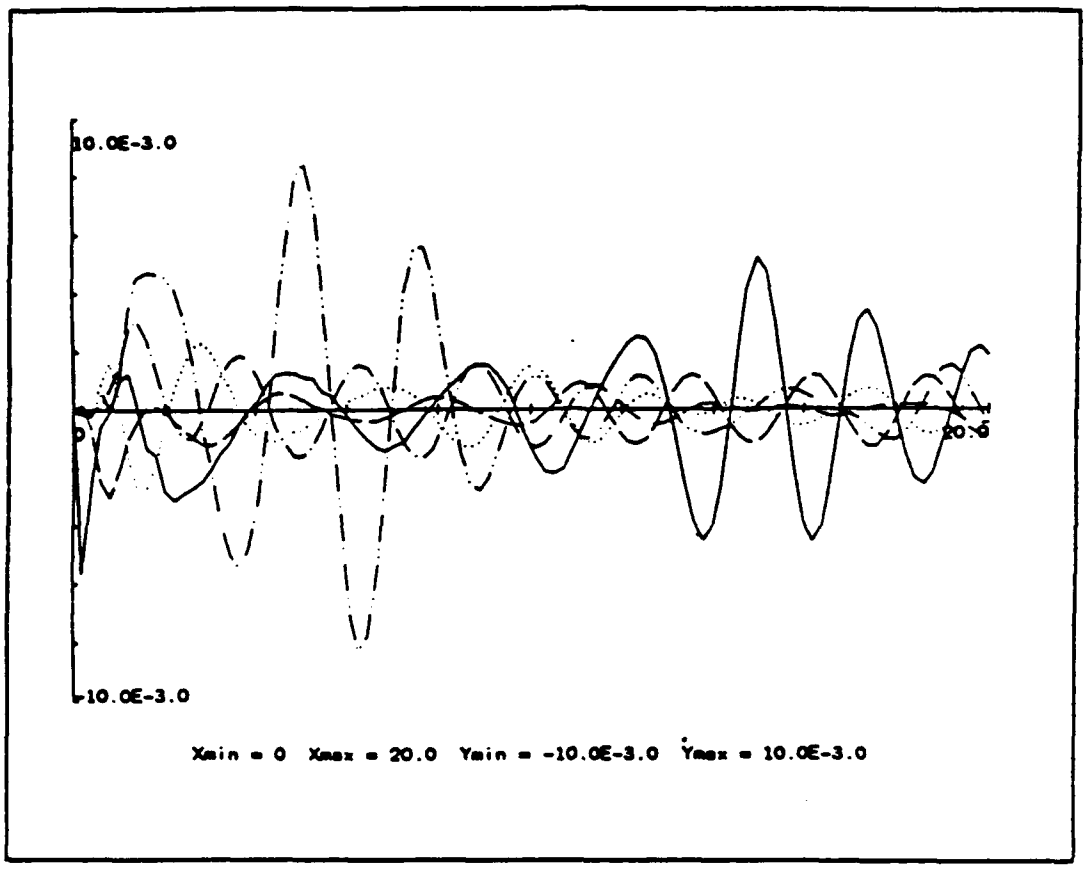

Legend

η = + 1.0
η = + 0.6
η = 0.0
η = - 0.6
η = - 1.0

Figure 8. Transient normal velocities at five locations on the shell: Additional data points would smooth out the plots.

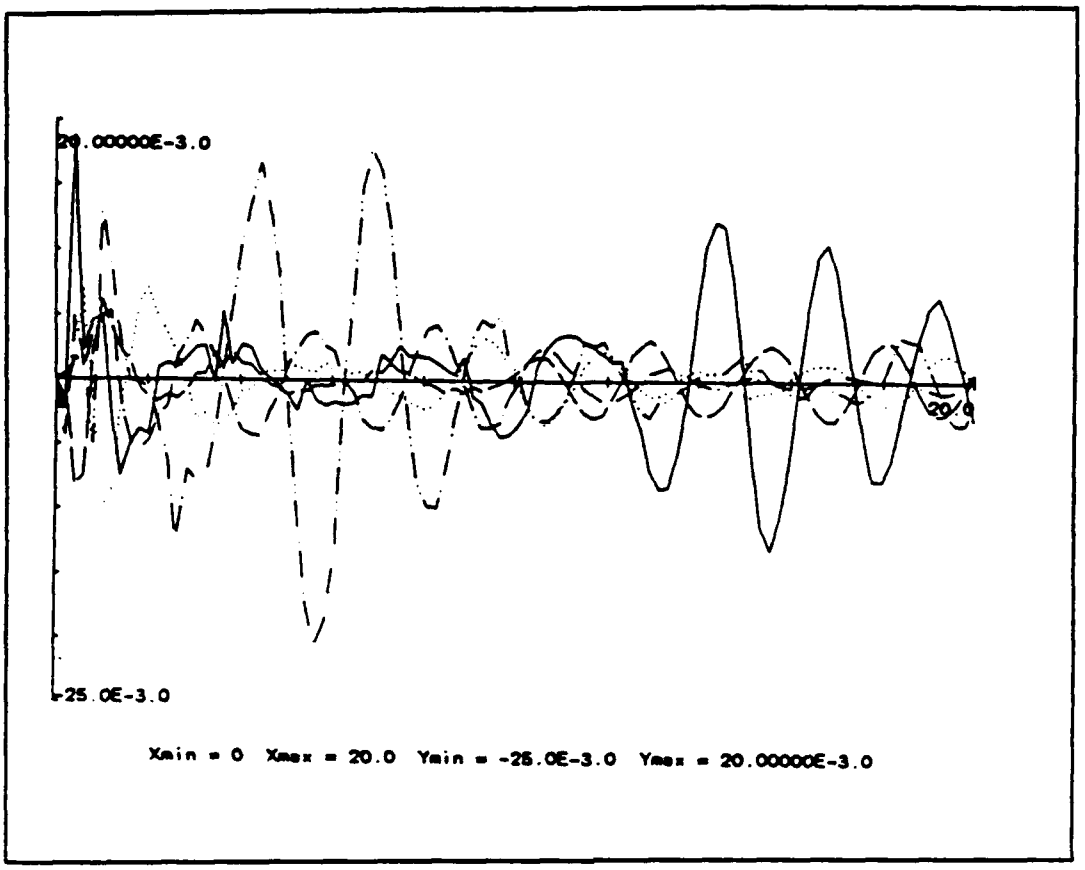

Legend

η = + 1.0
η = + 0.6
η = 0.0
η = - 0.6
η = - 1.0

Figure 9. Transient normal accelerations at five locations on the shell: Additional points would smooth out the plots.

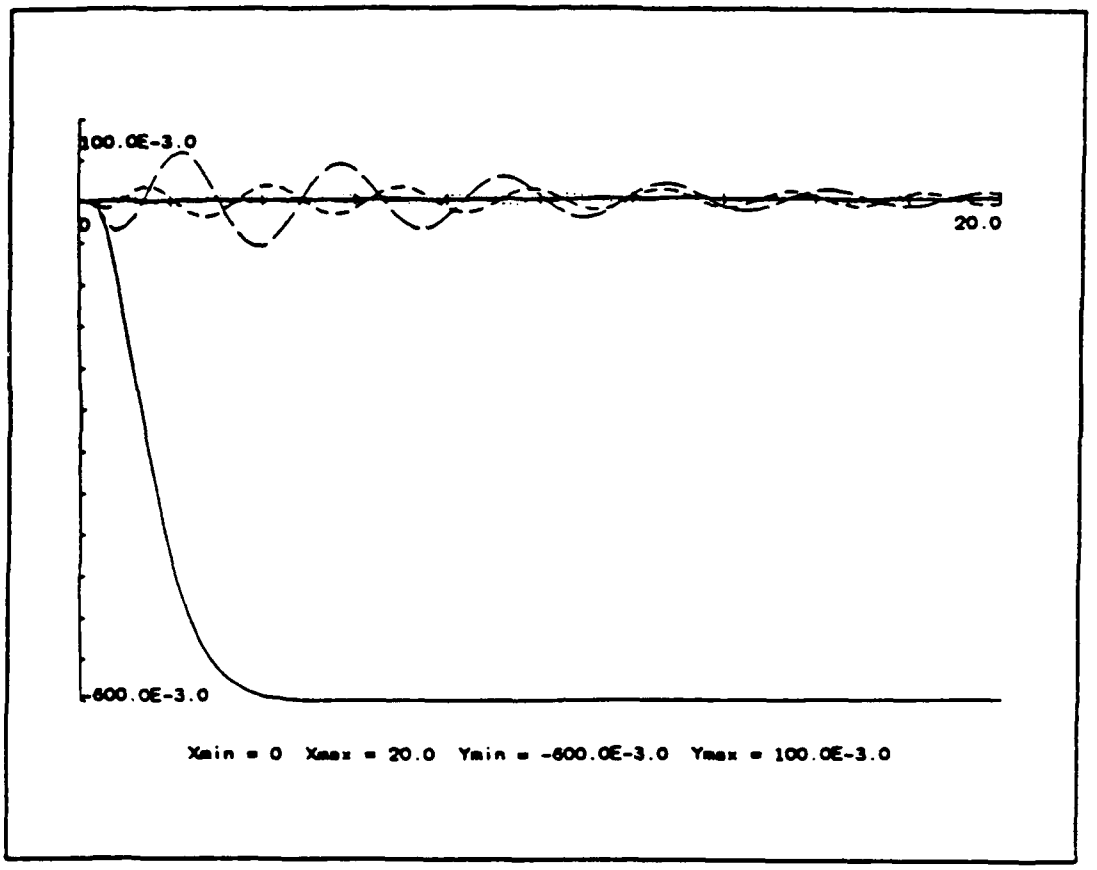

Legend

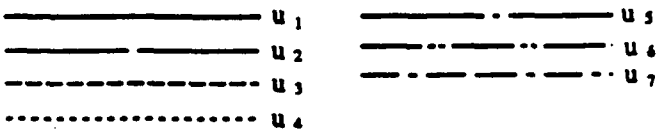

Figure 10. Modal time-dependent tangential amplitudes for m = 1 - 7: With the exception of component m = 1, the generalized displacements return to their original equilibrium position. However, the m = 1 contribution results in a finite displacement of the shell. Note that m = 0 is zero by definition.

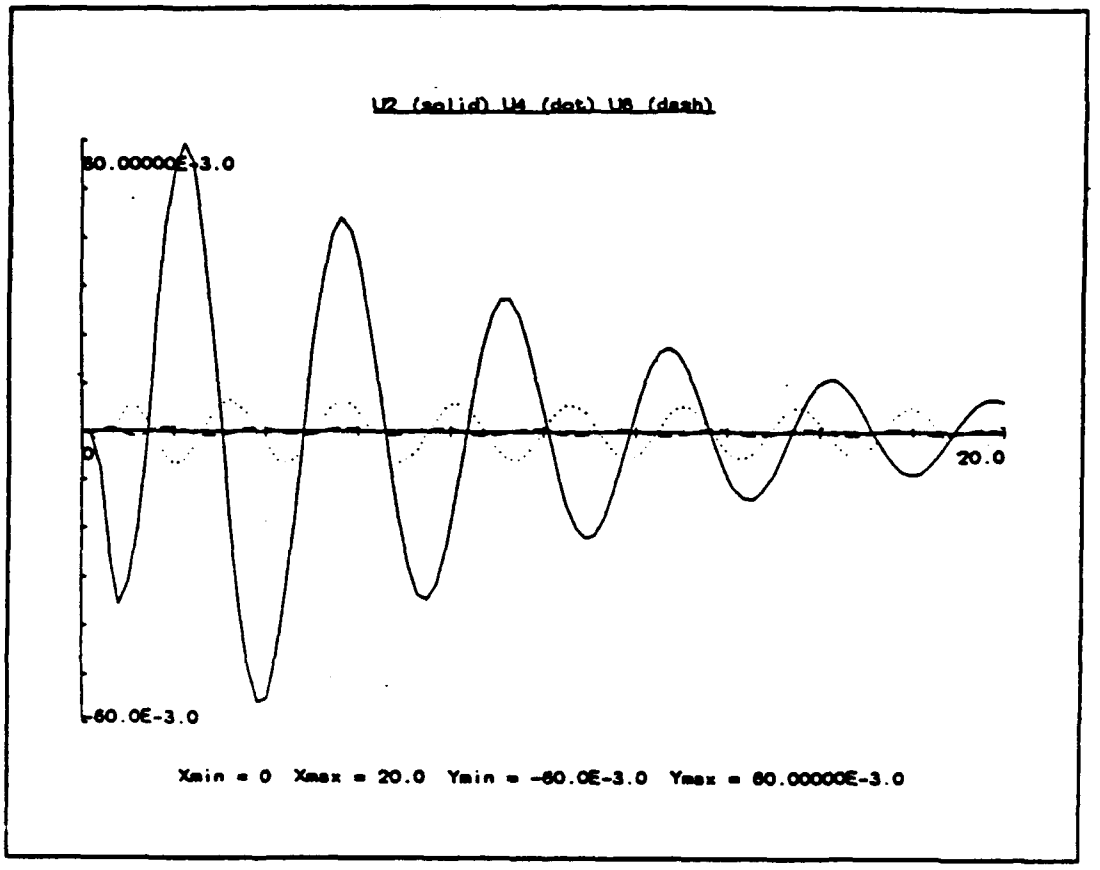

Figure 11. Transient tangential deflection coefficients for even m = 2 - 6: Note that the m = 2 mode has the most significant amplitude. This explains its strong coupling to the lower even modes.

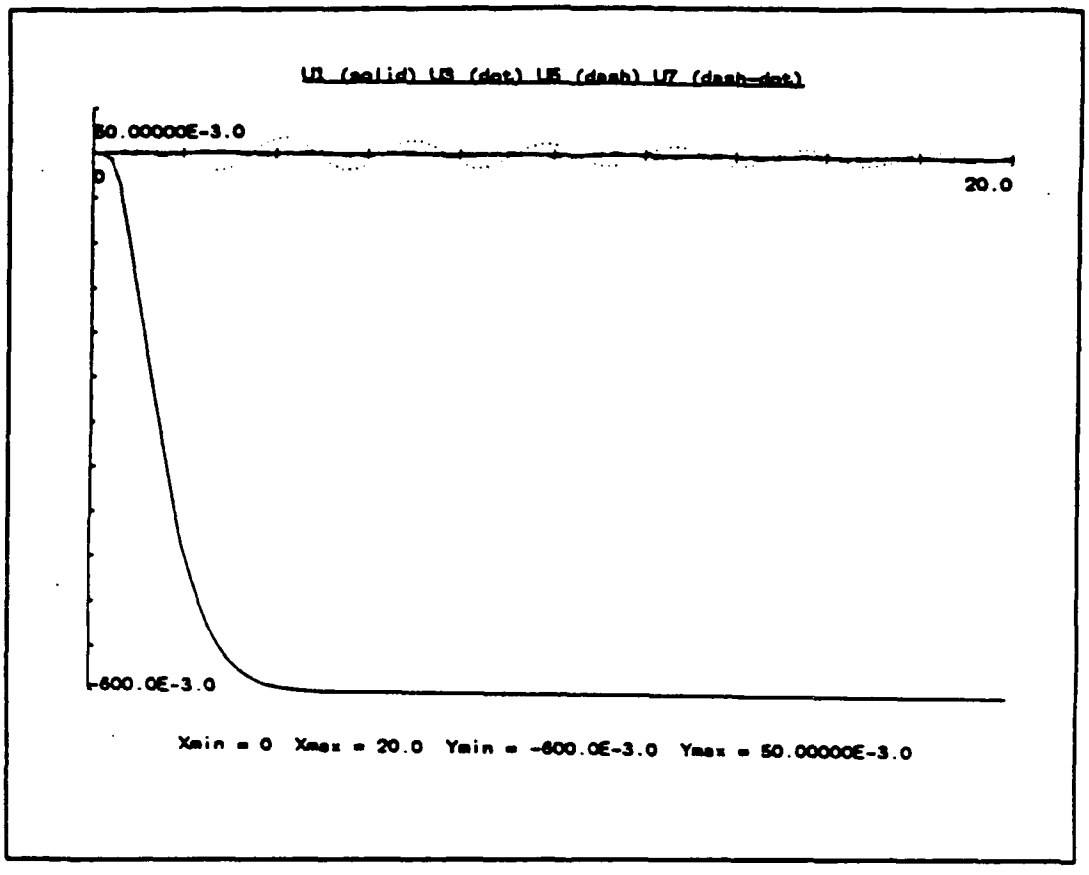

Figure 12. Transient tangential deflection coefficients for odd m = 1 - 7: The m = 1 mode finite displacement reflects the transfer of energy from the shell to the fluid in the form of radiation.

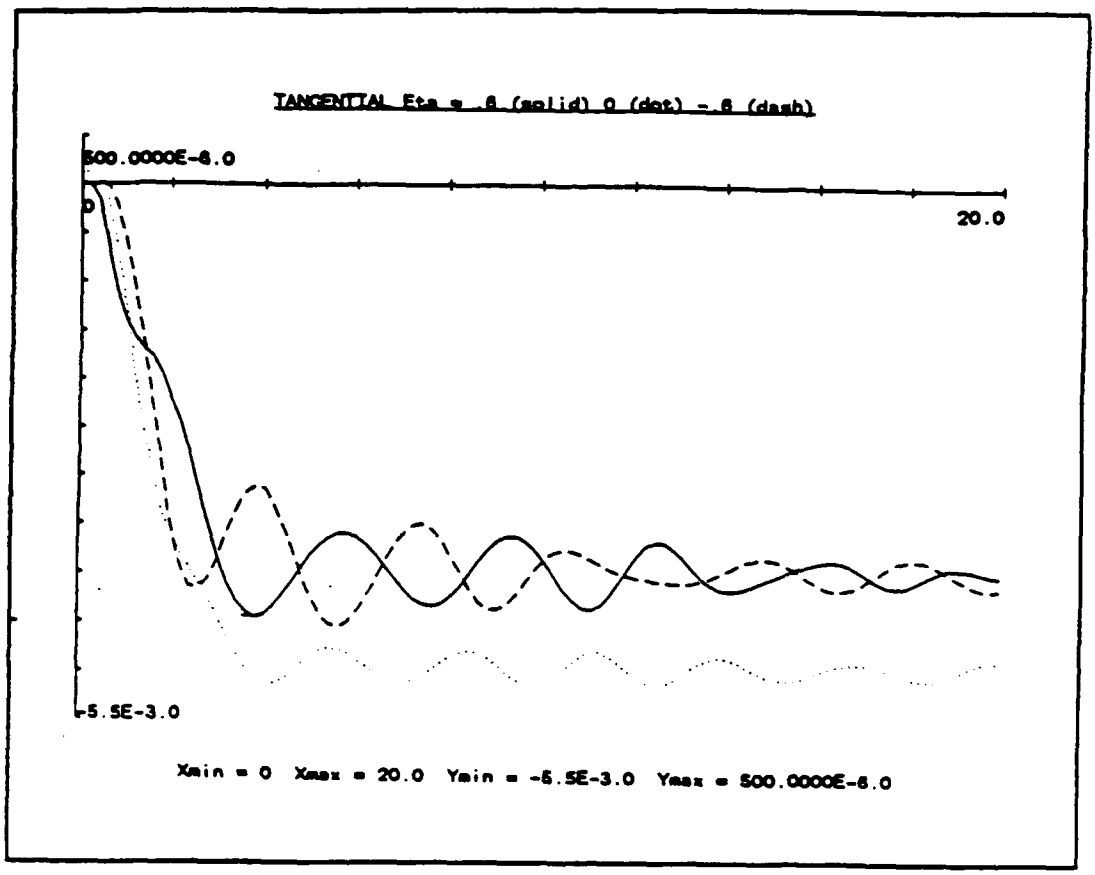

Figure 13. Early-time tangential displacements at three locations: The tangential displacements at the two vertices are zero.

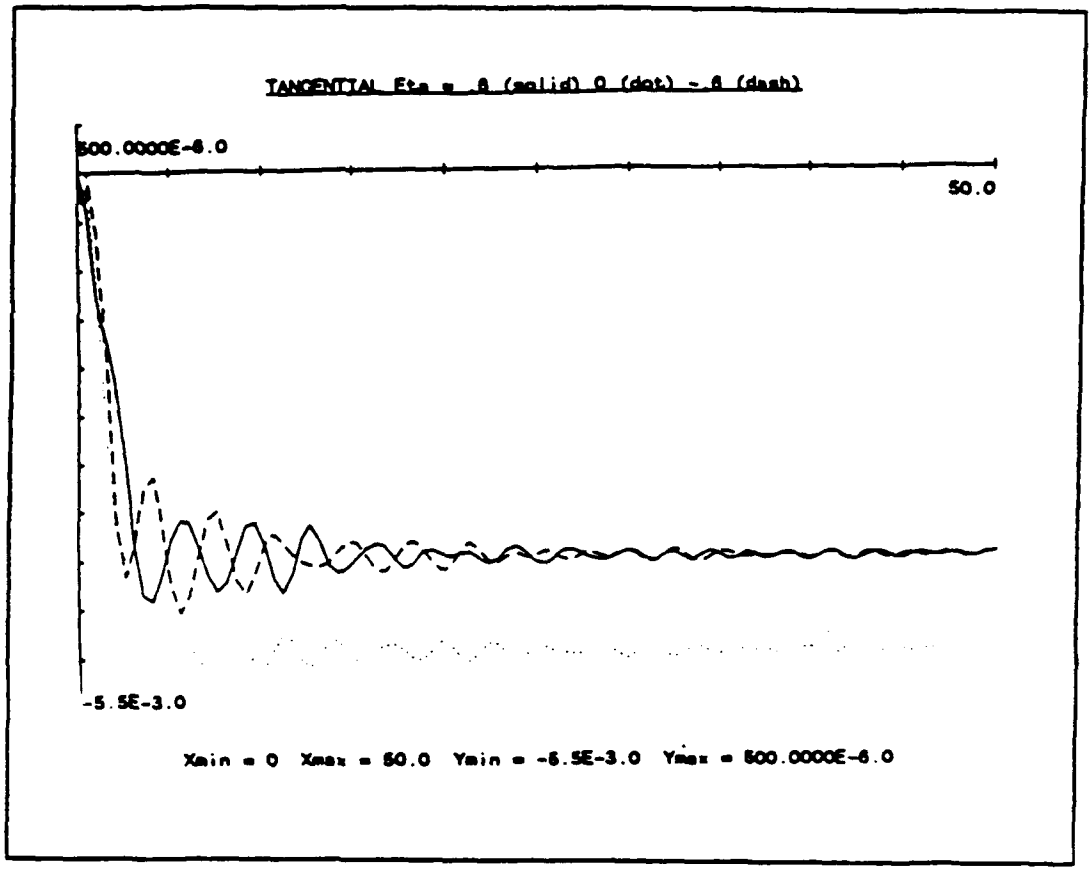

Figure 14. Longer-time tangential displacements at five locations: Note the oscillation of the displacement amplitudes—first dying out and then re-exciting, albeit to a lesser extent than was the case for the normal displacements.

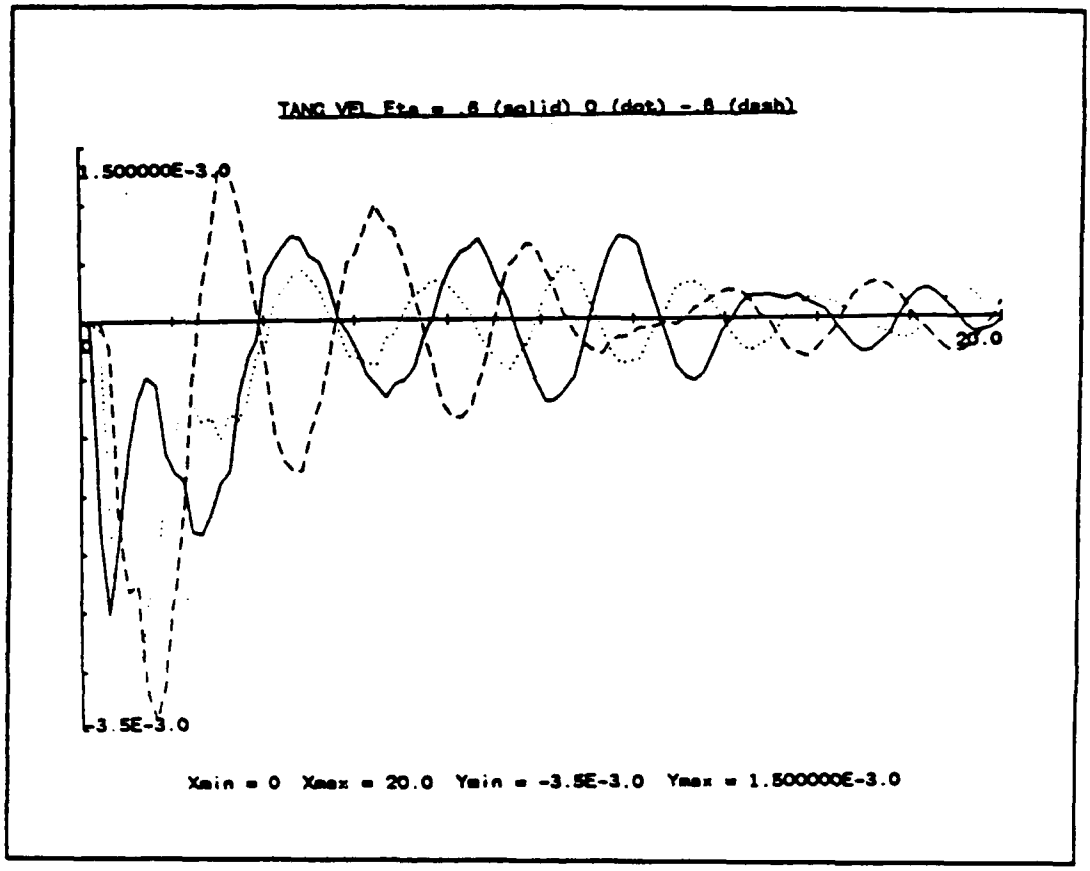

Figure 15. Transient tangential velocities at three locations on the shell: Additional data points would smooth out the plots.

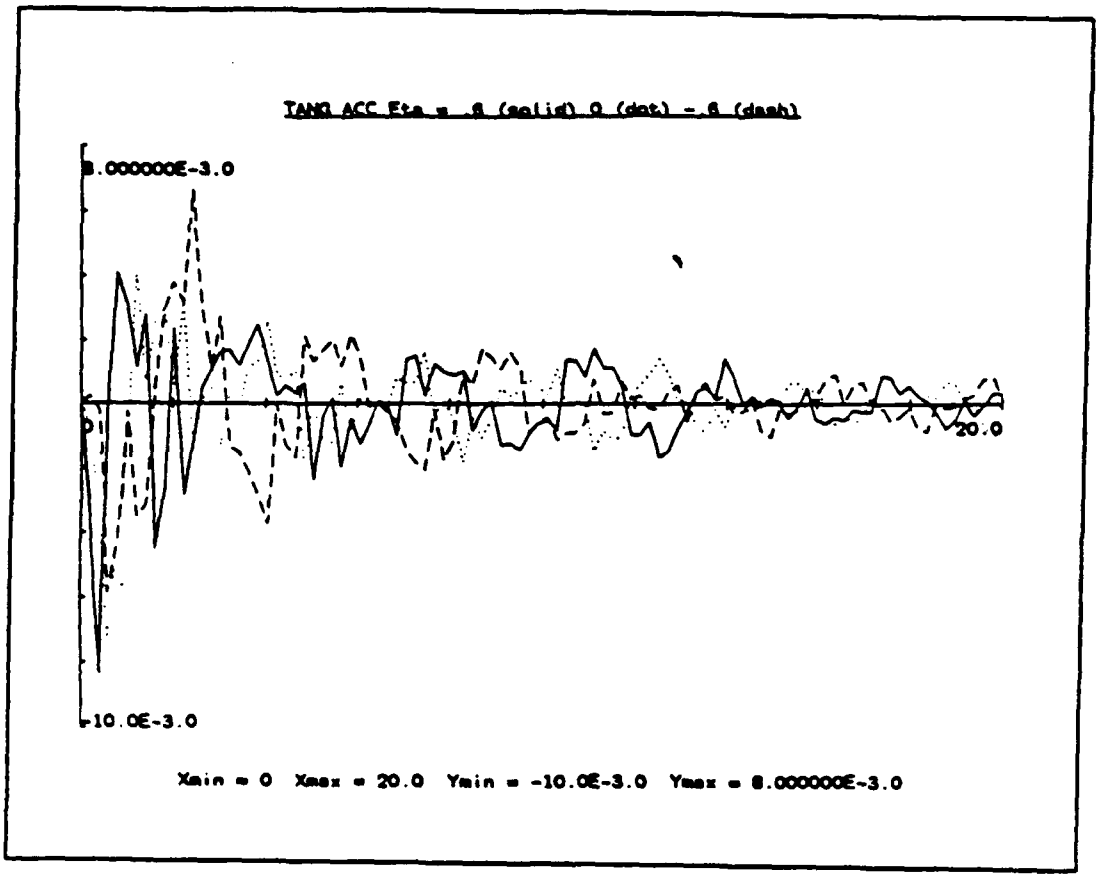

Figure 16. Transient tangential accelerations at three locations: Additional data points would smooth out the plots, and perhaps slightly increase the maximum values.

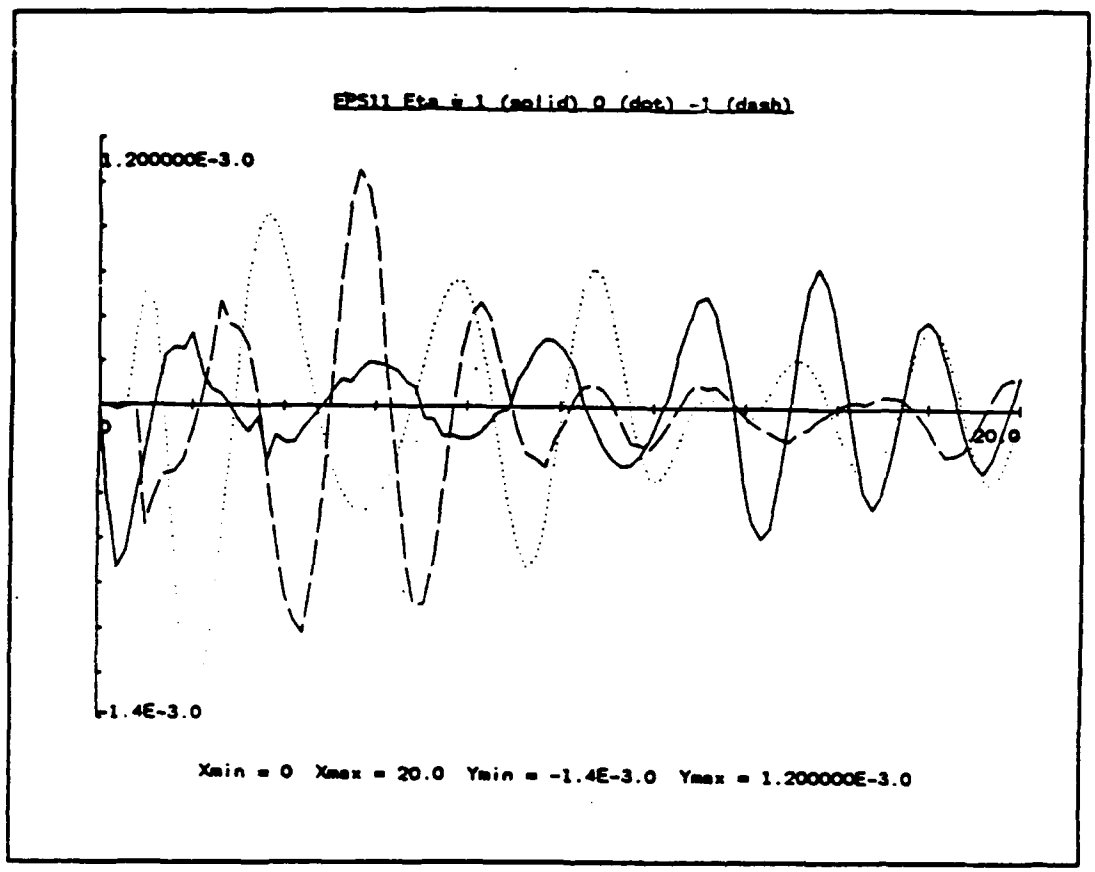

Figure 17. Strains in the ϕ-direction.

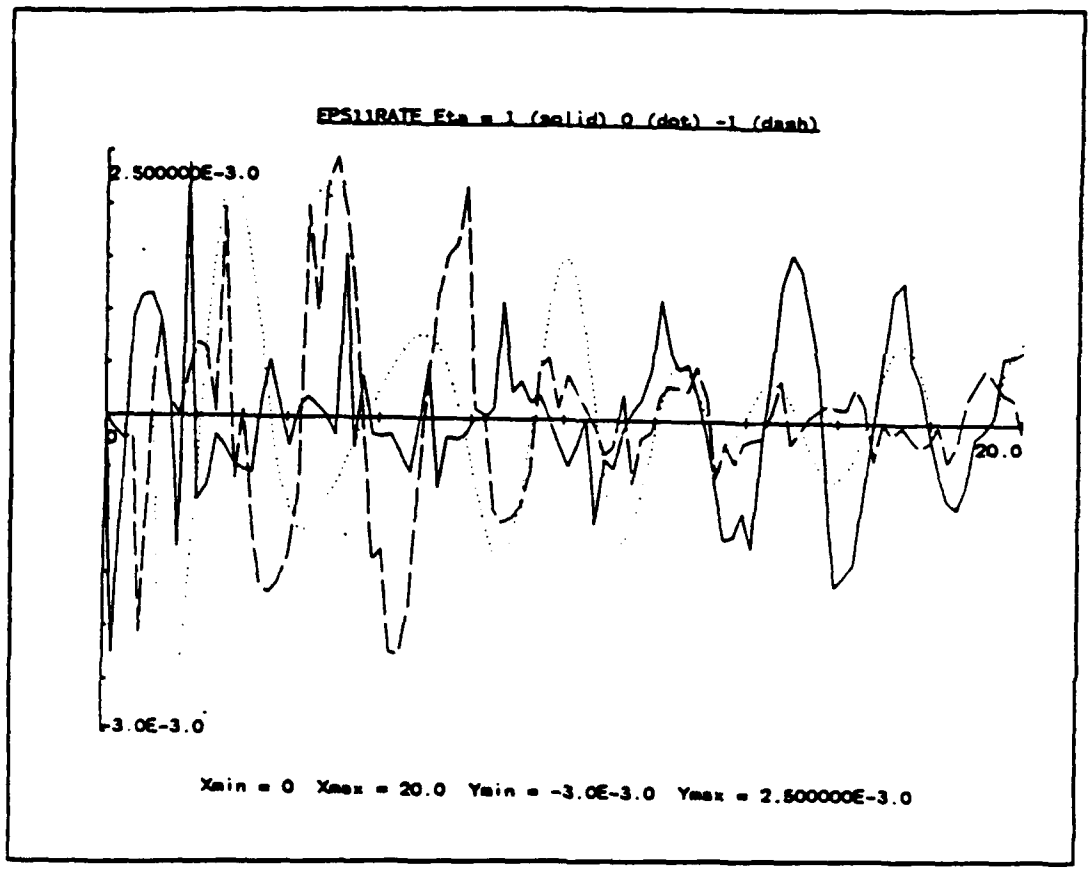

Figure 18. Strain rates in the ϕ-direction.

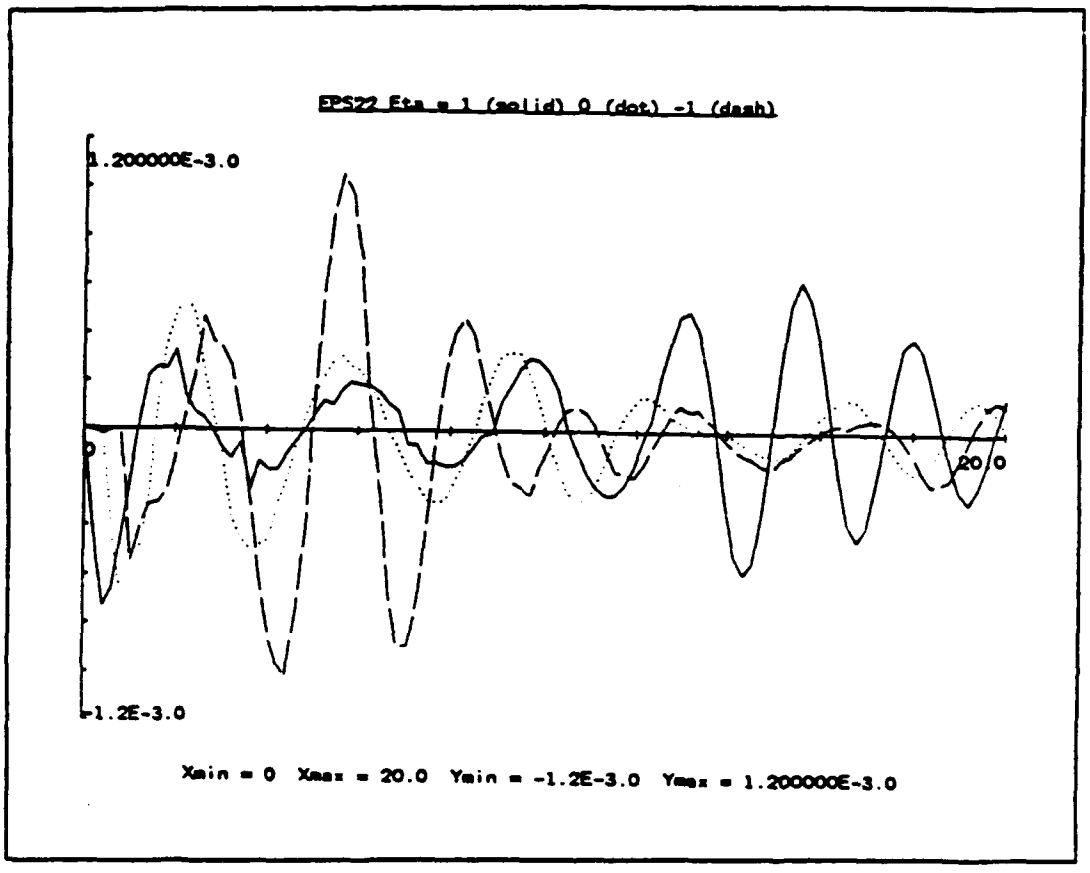

Figure 19. Strains in the η-direction.

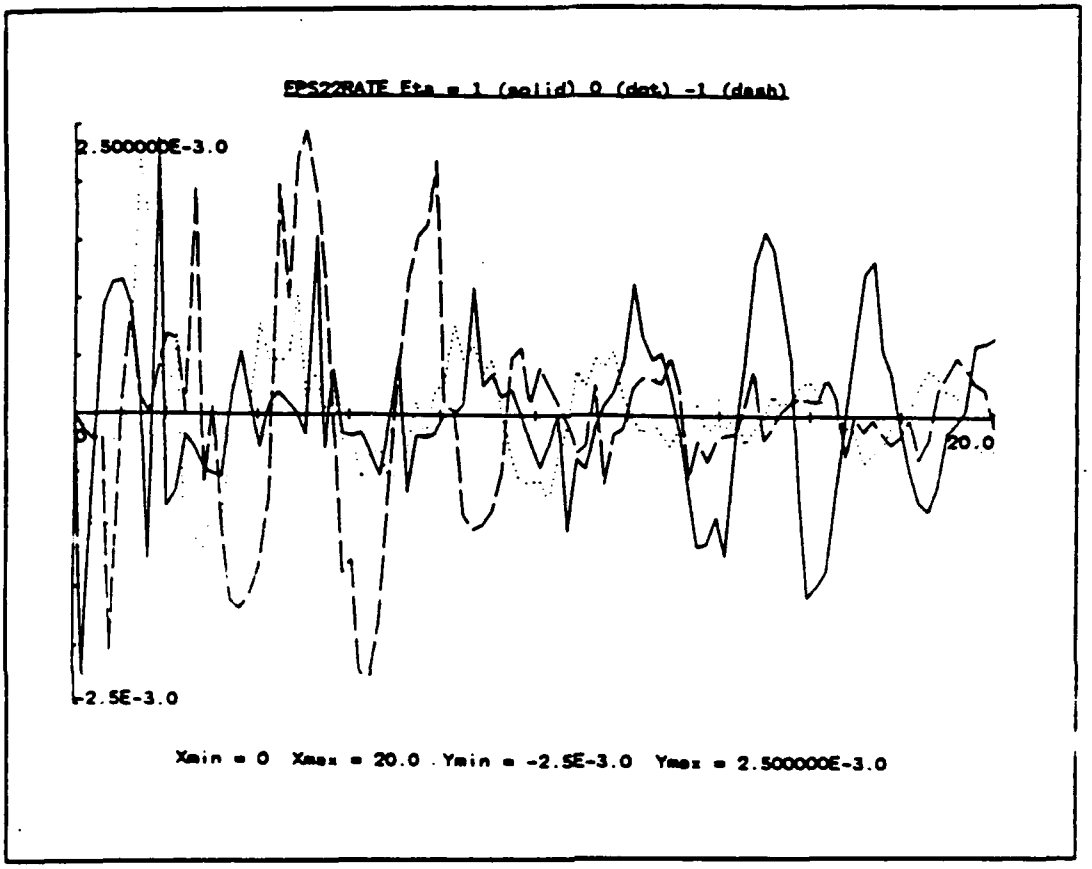

Figure 20. Strain rates in the η-direction.

3.4.2 Case II and Case III.

Reasonable numerical results could not be obtained for these cases. We believe that this did not result from a fundamental flaw in the theory. Rather, it is because the series solutions do not converge as fast as the aspect ration is increased. In addition, cross-coupling terms which were negligible in the first case are more important in these cases. If the model size that DOE-MACSYMA could handle were increased and more computer power were used, solution should be possible. This is not currently practical. However, as computer power expands in the future, it should become more reasonable.

SECTION 4

CONCLUSIONS

In order to solve the prolate spheroidal fluid-solid interaction problem, it was necessary to balance classical analysis and numerical code development. Separation of the prolate spheroidal wave equation reveals the prolate spheroidal angular and radial functions to be the exact solutions to the prolate spheroidal acoustic wave equation, as expected. The prolate spheroidal angular functions are also determined to be eigen solutions for the prolate spheroidal shell equilibrium equations. The shell displacement and fluid pressure fields are expressed in terms of an infinite series expansion using the complete set of prolate spheroidal angular functions and are therefore exact. The resulting expressions are very complex (Ref. 4, Chapter 5). However, DOE-MACSYMA was very helpful in dealing with the complex algebraic manipulations.

The final result was an exact solution for the transient response of both the prolate spheroidal shell and the surrounding fluid medium. However, the results are represented in terms of infinite series, embedded in infinite series, embedded in infinite series, etc. Computationally, such a representation is very difficult to deal with (Ref. 4, Chapter 5).

A novel trimming procedure, which was guided by the functional insight gained in the analysis, was required to solve for numerical answers. This trimming procedure was sufficient to obtain shock-loaded results for the nearly-spherical prolate spheroidal geometry (Ref. 4, Chapter 5). For this case, the results were compared with the results previously generated for the perfect sphere and the agreement was excellent.

Unfortunately, this procedure was not sufficient to obtain valid solutions for the higher eccentricity geometrics. One of the primary problems for the eccentric geometries is modal coupling. Unfortunately, the fact that the resulting series solutions are separately solutions to the wave equations and the shell equations does not mean that they are normal eigenfunctions which would uncouple the equations. Theoretically, a set of normal eigenfunctions exist which would uncouple the equations. However, it is not known how to find such a set of functions.

In principal, the equations can be evaluated in spite of the cross-coupling. However, it was determined that the higher the eccentricity, the slower the power series converged and the more significant the coupling of the modes. For practical solution with currently reasonable computer resources, the cross-coupling terms must be dropped and the series truncated at a reasonable number of terms. Unfortunately, this results in incorrect answers. In the future, increased computer power may make this

solution useful in an engineering sense. However, at this time the method can not be used to solve practical problems.

Since reasonable numerical solutions could not be obtained for high eccentricity geometries using the new closed-form theory, we were unable to compare the new theory with experimental or finite element results.

SECTION 5

LIST OF REFERENCES

1. Huang, Hanson, "Transient Interaction of Plane Acoustic Waves with a Spherical Elastic Shell," Journal of the Acoustical Society of America, Volume 45, No. 3, March 1969, pp. 661-670. (Unclassified)

2. Jones-Oliveira, Janet B., "Transient Interaction of Plane Acoustic Waves with Submerged Elastic Spherical Shells," Master of Science Thesis, Massachusetts Institute of Technology, CSDL-T-846, Revision A, June 1984. (Unclassified)

3. Jones-Oliveira, Janet B., and Peter J. Wender, "Explosive Shock Analysis and Test of a Sonar Towed Body," CSDL-P-1981, December 1984 [also published in The 55th Shock and Vibration Bulletin]. (Unclassified)

4. Jones-Oliveira, Janet Bughardt, "Fluid-Solid Interaction of a Prolate Spheroidal Shell Structure by an Acoustic Shock Wave," Doctoral Thesis, Massachusetts Institute of Technology, March 1990. (Unclassified)

5. Kraus, Harry, "Thin Elastic Shells," John Wiley and Sons, Inc., New York, NY, 1967, pp. 333-341. (Unclassified)

6. Nemergut, P.J., and R.S. Brand, "Axisymmetric Vibrations of Prolate Spheroidal Shells," Journal of the Acoustical Society of America, Volume 38, 1965, pp. 262-265. (Unclassified)

7. Pauwelussen, Poop P., "Validation of the Underwater Shock Analysis Program USA," Part II: Numerical Computations, Institute for Mechanical Constructions, January 1987. (Unclassified)

8. Shiraishi, N., and Frank L. DiMaggio, "Perturbation Solution for the Axisymmetric Vibrations of Prolate Spheroidal Shells," Journal of the Acoustical Society of America, Volume 34, 1962, pp. 1725-1731. (Unclassified)

9. Silbiger, Alexander, and Frank DiMaggio, "Extensional Axi-Symmetric Second Class Vibrations of a Prolate Spheroidal Shell," Office of Naval Research, Contract Nonr-266(67), Project 385-414, Technical Report No. 3, February 1961. (Unclassified)

DISTRIBUTION LIST

DNA-TR-90-171

DEPARTMENT OF DEFENSE

ASSISTANT TO THE SECRETARY OF DEFENSE
ATTN: EXECUTIVE ASSISTANT

DEFENSE INTELLIGENCE AGENCY
ATTN: DB-6E1
ATTN: DIW-4
ATTN: OGA-4B2

DEFENSE NUCLEAR AGENCY
ATTN: OPNS
ATTN: SPSD
ATTN: SPWE
ATTN: SPWE K PETERSEN
2 CYS ATTN: TITL

DEFENSE TECHNICAL INFORMATION CENTER
2 CYS ATTN: DTIC/FDAB

FIELD COMMAND DEFENSE NUCLEAR AGENCY
ATTN: FCPR

FIELD COMMAND DEFENSE NUCLEAR AGENCY
ATTN: FCNV

FIELD COMMAND DEFENSE NUCLEAR AGENCY
ATTN: FCNM

DEPARTMENT OF THE ARMY

DEP CH OF STAFF FOR OPS & PLANS
ATTN: DAMO-SWN

HARRY DIAMOND LABORATORIES
ATTN: SLCIS-IM-TL TECH LIB

U S ARMY CORPS OF ENGINEERS
ATTN: CERD-L

U S ARMY ENGR WATERWAYS EXPER STATION
ATTN: CEWES J K INGRAM
ATTN: CEWES-SD/DR J G JACKSON, JR
ATTN: J ZELASKO CEWES-SD-R
ATTN: R WHALIN CEWES ZT
ATTN: RESEARCH LIBRARY

U S ARMY NUCLEAR & CHEMICAL AGENCY
ATTN: MONA-NU DR D BASH

U S ARMY SPACE & STRATEGIC DEFENSE CMD
ATTN: CSSD-SA-EV
ATTN: CSSD-SL

U S ARMY WAR COLLEGE
ATTN: LIBRARY

USA SURVIVABILITY MANAGMENT OFFICE
ATTN: SLCSM-SE J BRAND

DEPARTMENT OF THE NAVY

DAVID TAYLOR RESEARCH CENTER
ATTN: CODE 172
ATTN: CODE 173
ATTN: CODE 1740
ATTN: CODE 1750
ATTN: CODE 1770
ATTN: CODE 2740

MARINE CORPS
ATTN: CODE POR-21

NAVAL COASTAL SYSTEMS CENTER
ATTN: CODE 7410

NAVAL DAMAGE CONTROL TRAINING CENTER
ATTN: COMMANDING OFFICER

NAVAL ELECTRONICS ENGRG ACTVY, PACIFIC
ATTN: CODE 250

NAVAL EXPLOSIVE ORD DISPOSAL TECH CENTER
ATTN: CODE 90 J PETROUSKY

NAVAL POSTGRADUATE SCHOOL
ATTN: CODE 1424 LIBRARY

NAVAL RESEARCH LABORATORY
ATTN: CODE 2627 TECH LIB

NAVAL SEA SYSTEMS COMMAND
ATTN: SEA-08
ATTN: SEA-423
ATTN: SEA-511
ATTN: SEA-55X1
ATTN: SEA-55Y

NAVAL SURFACE WARFARE CENTER
ATTN: CODE H21
ATTN: CODE R14
ATTN: CODE R15

NAVAL WEAPONS CENTER
ATTN: CODE 3241 D HERIGSTAD

NAVAL WEAPONS EVALUATION FACILITY
ATTN: CLASSIFIED LIBRARY

NEW LONDON LABORATORY
ATTN: TECH LIBRARY

OFFICE OF CHIEF OF NAVAL OPERATIONS
ATTN: NOP 091
ATTN: NOP 223
ATTN: NOP 225
ATTN: NOP 37
ATTN: NOP 605D5
ATTN: NOP 957E
ATTN: OP 03EG
ATTN: OP 21
ATTN: OP 654
ATTN: OP 73 TAC READINESS DIV

OFFICE OF NAVAL RESEARCH
ATTN: CODE 1132SM
ATTN: CODE 23

DEPARTMENT OF THE AIR FORCE

AIR FORCE INSTITUTE OF TECHNOLOGY/EN
ATTN: COMMANDER

HQ USAF/CCN
ATTN: AFCCN

UNITED STATES STRATEGIC COMMAND
ATTN: J 51
ATTN: J 533
ATTN: J 534
ATTN: J 535

DEPARTMENT OF ENERGY

LAWRENCE LIVERMORE NATIONAL LAB
ATTN: D MAGNOLI

LOS ALAMOS NATIONAL LABORATORY
ATTN: REPORT LIBRARY
ATTN: TECH LIBRARY

MARTIN MARIETTA ENERGY SYSTEMS INC
ATTN: DR C V CHESTER

SANDIA NATIONAL LABORATORIES
ATTN: TECH LIB 3141

U S DEPARTMENT OF ENERGY
OFFICE OF MILITARY APPLICATIONS
ATTN: OMA/DP-252 MAJ D WADE

OTHER GOVERNMENT

CENTRAL INTELLIGENCE AGENCY
ATTN: OSWR/NED

DEPARTMENT OF DEFENSE CONTRACTORS

ANALYSIS & TECHNOLOGY INC
ATTN: V GODINO

APPLIED RESEARCH ASSOCIATES, INC
ATTN: R FRANK

CALIFORNIA INSTITUTE OF TECHNOLOGY
ATTN: T AHRENS

CALIFORNIA RESEARCH & TECHNOLOGY, INC
ATTN: J THOMSEN
ATTN: K KREYENHAGEN

CHARLES STARK DRAPER LAB, INC
2 CYS ATTN: D S NOKES

COLUMBIA UNIVERSITY
ATTN: F DIMAGGIO

KAMAN SCIENCES CORP
ATTN: LIBRARY

KAMAN SCIENCES CORP
ATTN: DASIAC
ATTN: E CONRAD

KAMAN SCIENCES CORPORATION
ATTN: DASIAC

KARAGOZIAN AND CASE
ATTN: J KARAGOZIAN

LOCKHEED MISSILES & SPACE CO, INC
ATTN: PHILIP UNDERWOOD

LOCKHEED MISSILES & SPACE CO, INC
ATTN: TECH INFO CTR

PACIFIC-SIERRA RESEARCH CORP
ATTN: H BRODE

S-CUBED
ATTN: K D PYATT, JR
ATTN: R SEDGEWICK

SCIENCE APPLICATIONS INTL CORP
ATTN: TECHNICAL REPORT SYSTEM

TELEDYNE BROWN ENGINEERING
ATTN: J RAVENSCRAFT

TITAN CORPORATION
ATTN: LIBRARY
ATTN: S SCHUSTER

WEIDLINGER ASSOC, INC
ATTN: H LEVINE

WEIDLINGER ASSOCIATES, INC
ATTN: T DEEVY

WEIDLINGER ASSOCIATES, INC
ATTN: M BARON

WESTINGHOUSE ELECTRIC CORP
ATTN: D BOLTON ADV DEVELOP